ROOM AND ELEVATED TEMPERATURE SLIDING WEAR BEHAVIOR OF COLD SPRAYED Ni-WC COMPOSITE COATINGS

Tyler B. Torgerson, B.S.

Thesis Prepared for the Degree of

MASTER OF SCIENCE

UNIVERSITY OF NORTH TEXAS

August 2018

APPROVED:

Thomas W. Scharf, Major Professor
Samir Aouadi, Committee Member
Andrey Voevodin, Committee Member and Chair of the Department of Materials Science and Engineering
Yan Huang, Interim Dean of the College of Engineering
Victor Prybutok, Dean of the Toulouse Graduate School

Torgerson, Tyler B. *Room and Elevated Temperature Sliding Wear Behavior of Cold Sprayed Ni-WC Composite Coatings*. Master of Science (Materials Science and Engineering), August 2018, 50 pp., 4 tables, 20 figures, 40 numbered references.

The tribological properties of cold sprayed Ni-WC metal matrix composite (MMC) coatings were investigated under dry sliding conditions from room temperature (RT) up to 400°C, and during thermal cycling to explore their temperature adaptive friction and wear behavior. Characterization of worn surfaces was conducted using scanning electron microscopy (SEM), energy dispersive spectroscopy (EDS), and Raman spectroscopy to determine the chemical and microstructural evolution during friction testing. Data provided insights into tribo-oxide formation mechanisms controlling friction and wear. It was determined that the steady-state coefficient of friction (CoF) decreased from 0.41 at RT to 0.32 at 400˚C, while the wear rate increased from 0.5×10-4 mm3/N·m at RT to 3.7×10-4 mm3/N·m at 400˚C. The friction reduction is attributed primarily to the tribochemical formation of lubricious NiO on both the wear track and transfer film adhered to the counterface. The increase in wear is attributed to a combination of thermal softening of the coating and a change in the wear mechanism from adhesive to more abrasive. In addition, the coating exhibited low friction behavior during thermal cycling by restoring the lubricious NiO phase inside the wear track at high temperature intervals. Therefore, cold sprayed Ni-WC coatings are potential candidates for elevated temperature and thermally self-adaptive sliding wear applications.

ACKNOWLEDGEMENTS

My appreciation and gratitude goes to my distinguished advisor Thomas W. Scharf. You are an excellent teacher, a renowned tribologist and, most importantly, a great mentor. Thank you for the profound experience and opportunities that you provided me in the form of academic research and networking. To Drs. Voevodin and Aouadi, thank you for your notable contributions to this thesis and serving as committee members. To the MTSE department staff, including the supervisors of MRF, thank you for your time, knowledge and vast resources that you provided throughout my materials science courses and graduate research endeavors. Thank you to Jon-Erik Mogonye and Jonova Thomas for their invaluable advice during training on the testing and characterization equipment. I want to give a special thanks to Avery Young, Kiersten Tafoya and Jordan Reed, my fellow Grad Track peers and friends. Without their encouragement and influence, my undergraduate years would have been much less fulfilling. To my younger brother, Kyle, thank you for all of your support. We have been through so much together, and I am grateful that we are so close. You are a great brother and friend, I love you. To my mother and father, I love y'all more than anything and I am blessed for the strength and wisdom that y'all have imparted onto me throughout my life. It has been a unique journey to this point filled with obstacles and challenges, which we always persevered through. Thank you for your endless support, advice and constructive criticism which kept me humble. I love you both dearly. Finally, thank you to God and Jesus Christ my Lord and Savior, I would not be the man I am today without you in my life.

TABLE OF CONTENTS

Page

LIST OF TABLES

Page

LIST OF FIGURES

Page

CHAPTER 1

INTRODUCTION

1.1 Brief History of Tribology

Tribology is the science of interacting bodies in relative motion to one another which is defined by lubrication, friction and wear of interacting materials. The field, which was formally developed around 50 years ago, is marked by vast improvements in energy efficiency and functionality in moving mechanical assemblies (e.g. MEMS, bearing, engines, etc.), which has led to technological and societal innovations since the industrial revolution. However, this field has been acknowledged since ancient times dating back to the Greeks (where the word Tribology is derived) and Egyptians who poured water underneath sleds for lubrication purposes to move large building stones. Starting around the 1500's, during the renaissance age, experimentalists began to postulate theories of friction. Leonardo da Vinci was the first to presuppose the concept of coefficient of friction, i.e. the ratio of frictional force to normal force, and also concluded that friction is independent of the contact area [5]. While, Beauchamp Tower in 1883 found that a thin fluid film forms at the interface, preventing contact, called hydrodynamic lubrication, and Reynolds further confirmed the theory and developed the well-known Reynolds equation [1-2]. Later, junction growth theory and adhesion theory of friction (Bowden and Tabor) in the 1950s were introduced and further improved, which provided a foundation for predicting and further understanding frictional properties and behavior of contact bodies [1-2,5]. Today, no theories of friction can accurately predict the coefficient of friction for any dry sliding pair without adding questionable assumptions due to the large amount of dependent parameters that influence the effects as well as the inherent complexity of mixing interfaces. Thus, there is still much to learn and understand about the role of different materials and their corresponding wear behavior.

1.2 Motivation

Most mechanical moving systems and assemblies are composed of metal-base components that require some form of lubrications during operation. Solid lubricants are used on moving mechanical assemblies in place of oil-base lubricants in low/high temperature environments and extreme pressure conditions. They are typically used on machining equipment, bearings, gears, aerospace components, air compressors and fasteners. Because of adhesion issues, chemical degradation, evaporation and thermal expansion effects [1-2,7], solid lubricants such as MoS_2 and WS_2 (transition metal dichalcogenides), carbon-based materials (e.g. graphite and diamond-like carbon, or DLCs), soft metals, ceramics, and novel composite coatings are being investigated to address these specific problems. Graphite is the typical solid lubricant thought of for dry sliding and/or rolling due to its characteristic layered hexagonal structure ($P\text{-}6_3/mmc$). The carbon atoms experience covalent bonding in the basal plane, while the basal planes are attracted by weak Van der Waals cohesive forces, resulting in low interplanar shearing where planes easily slide over one another by intracrystalline slip [4]. Due to basal planes becoming damaged during sliding, reactive sites are exposed that require the presence of water or oxygen in the environment to promote lubrication (through interlamellar shearing) by passivation of the high energy edge sites [1], thereby avoiding adhesion problems with contacting bodies. DLC is another common and more prevalent solid lubricant for engineering applications. DLC coatings are generally amorphous with some short range ordering of sp3-type tetrahedral bonding (diamond hybridization) and sp2-type trigonal bonding (graphitic hybridization), which promotes a low coefficient of friction and wear rates with relatively high hardness [4]. An added benefit of DLCs is their tribological properties can by tailored by using different processing techniques, such as laser and (chemical or physical) vapor deposition, and controlling the chemical bonding through hydrogen content which allows

for DLCs to be used in both humid or dry (and inert) environment. Another group of solid lubricants termed transition metal dichalcogenide (TMDs) (e.g. MoS_2) whose lubrication behavior is similar to graphite with an intrinsically lubricious (hexagonal) structure. However, in this case, the bonding within the S-Mo-S layer is covalent, which act as the 'sandwiched' basal plane during sliding by intracrystalline slip and promotes the formation of a transfer film onto the counterface to accommodate interfacial sliding, i.e. the transfer film induces low friction [1,4]. Unlike graphite, TMDs function in dry inert gas or in ultrahigh vacuum; when exposed to ambient air, TMDs will undergo tribooxidation from unsaturated bonds on the edge of the basal planes, forming MoO_3 and WO_3, which leads to higher friction and a shorter wear life. Soft metals (e.g. Pb, In, Sn, etc.) are used as solid lubricant as well. By applying these coatings to a hard substrate, during sliding or rolling, a thin layer of the soft metal that does not transfer to the counterface will act to accommodate stress, and, in addition, their relatively low melting temperature can result in melt lubrication at asperity contacts [4]. It should be mentioned as well that specific polymers (PTFE), halides (CaF_2), sulfides ($BaSO_4$) and oxides (WO_3, TiO_2, Cr_2O_3, etc.) are also known to be acceptable solid lubricants. However, these solid lubricant mentioned above only function in a certain range of condition before their lubricative effects fail due to a change in bonding or structure from the environment and/or induced forces.

Defense departments (e.g. ARL, AFRL, NRL, etc.) are investigating novel solid lubricants and corresponding processing techniques that will provide functional coatings which are exposed to a multitude of different environments/conditions during operation, and thereby can be applied to next generation technology and warfare. Many of the aerospace and ground vehicles contain a component composed of a Ni-base alloy. These metals components and their respective lubricants/coatings are commonly processed using conventional processing techniques such as

vapor deposition and thermal spray due to reliability and efficiency; however, there are inherent problems associated with these techniques. In this study, a Ni-WC composite coating was investigated using a novel processing method. Ni-WC is a metal matrix composite with high hardness, toughness, wear resistance, and is commonly processed through thermal spray techniques (e.g. laser cladding). However, thermal spray processes occur at high temperatures generating concerns of phase changes, inhomogeneity of particle density, and residual stresses. Cold spray (CS) deposition is an alternative to thermal sprays, which may avoid such problems. This process accelerates particles in a gas, at temperatures below melting, through a de Laval nozzle obtaining supersonic velocities (300-1200m/s) prior to impact on substrate to prevent the concerns mentioned. Previous room temperature dry sliding wear tests on cold sprayed Ni-WC coatings reported room temperature steady-state coefficient of friction (COF) of 0.71, a wear rate of 0.1 $\times 10^{-4}$ $mm^3/N \cdot m$, and a wear behavior characterize by mechanically mixed tribolayers composed of nanocrystalline wear debris. However, there are no studies on CS Ni-WC coatings at high temperatures with a potential applications for bearing houses due to oxidation related problems with AISI 440C and M50 bearing steels around 400°C. Analysis of Ni based materials clearly indicate that these systems are capable of temperature adaptive behavior through the formation of low friction NiO phases, adding to the family of lubricious binary oxides reported in recent reviews [7,19-20]. Therefore, this study's aim is to investigate the dry sliding wear behavior and mechanisms of cold sprayed Ni-WC composite coatings at elevated temperatures. Specifically, a pure Ni and Ni-WC composite coating were tested under unidirectional dry sliding conditions at room temperature, 200°C, 400°C, and during thermal cycling with these temperatures. The effects of thermal softening, tribochemical phase formation, and microstructural evolution were evaluated at elevated temperatures to elucidate phenomena controlling friction and wear mechanisms.

1.3 Objectives

This thesis attempts to provide fundamental mechanistic insights in the following topics:

1. Understand cold sprayed Ni-WC sliding wear behavior and mechanisms at high temperature based on the friction and wear behavior, and the corresponding tribochemical phases that form.

2. Compare the sliding wear behavior of a Ni-WC coating cold sprayed at 800°C to understand the influence of processing temperature and the retention of WC particles.

3. Determine the effects of sliding counterface on the friction, wear rate, and chemical phases observed in wear.

1.4 Thesis Overview

There are 6 chapters composing this thesis that investigate the processing-structure-tribological property relationship of a cold sprayed Ni-WC composite coating. Chapter 1 gives an overview of cold spray solid lubricants and the tribological properties at elevated temperatures along with the motivation for this study. Chapter 2 provides an overview and insight into tribology, friction, dry sliding wear, solid lubricant coatings, and the benefits of cold spray. Chapter 3 gives a detailed explanation of experimental procedures of processing, wear tests and characterization of the cold spray coatings. Chapter 4 is the results and discussion of the processing-structure-property relationships for the as-deposited coatings and their corresponding tribological properties. The thesis concludes with Chapter 5 and 6 which summarizes the key topics addressed in this study and recommendations for future work.

CHAPTER 2

BACKGROUND

2.1 Tribology

Tribology is the science of interacting surfaces (the contact mechanics) in relative motion to one another with a basis on the mechanisms of lubrication, friction and wear. From these interactions, dissipation and transfer of stresses will occur at the interface in the form of physical (mechanical) deformation and chemical reactions, which can either protect or destroy contacting surfaces. In all varieties of human society such as biomedical, electronics, transportation, engineering, etc., there involves contacting surfaces which require protection in vastly different conditions. Figure 2.1 shows examples of different contact interactions in relative motion.

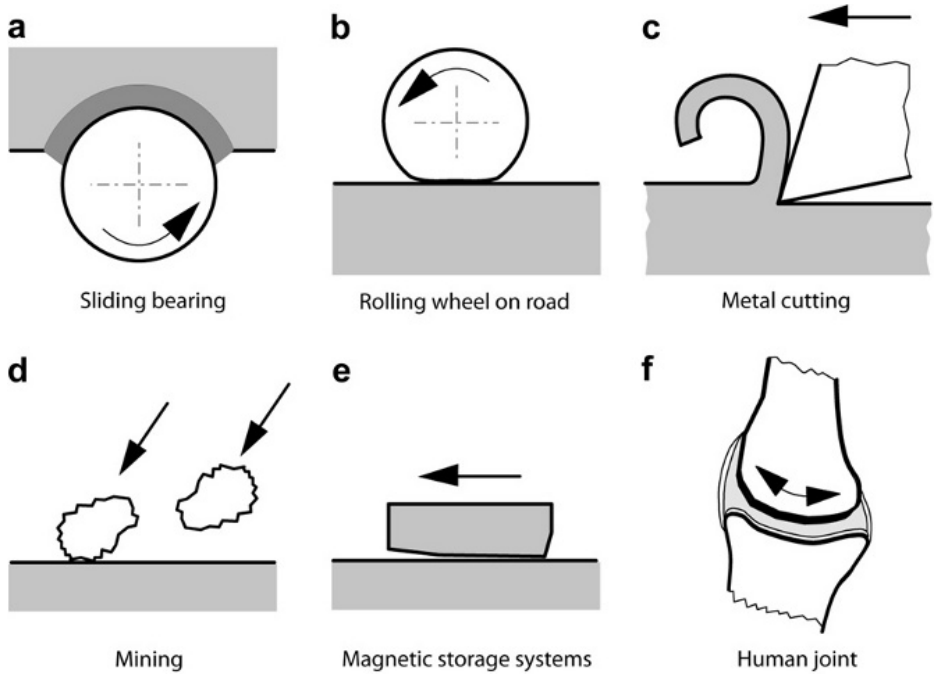

Figure 2.1: Examples of contact interactions during (a) sliding, (b) rolling, (c) cutting, (d) mining, (e) magnetic storage, and (f) joints. [3]

Thus, the evolution of tribology and surface engineering ultimately drive the advancement of society and technological progression as almost all applications involve some form of

interacting surfaces in relative motion which must be accounted for during design.

2.1.1 Solid State Friction

Friction is the resistance of one solid body sliding against another. For all lubricated components, the specific application and environment dictate the corresponding friction behavior and lubricant chosen. Moreover, the operating parameters during dry sliding, i.e. speed, load, temperature, humidity and topography of surface contract, are aspects that control the material's coefficient of friction (CoF) [1-3]. While a single CoF value for a given set of condition is adequate, values over a range of conditions is more realistic for industrial and defense applications as they are exposed to varying environments throughout operation. More importantly though, the behavior must be predictable (i.e. steady-state) and not cause vibrations [1] in order to avoid unexpected failures. The relatively magnitude of friction is, in general, expressed in terms of the CoF ($\mu = F/W$) where F is the frictional (sliding) force or load and W is the normal (static) force of the contacting bodies. The CoF was further expanded with the classical theory of Bowden and Tabor shown in Eq. 2.1

$$\mu = \frac{F}{W} = \frac{A_r * \tau}{W} = \frac{\tau}{P_H} = \frac{\tau_o}{P_H} + \alpha \quad (2.1)$$

where A_r is the real contact area, τ_0 is the interfacial shear strength, a "velocity accommodation parameter", and α expresses the pressure dependence of the shear strength. According to the theory, the CoF is a product of real contact area and the shear strength of the lubricant divided by the normal load or the ratio of shear strength to pressure if both forces are divided by the contact area [4]. This was shown to be accurate for a hard surface contacting a soft surface due to a reduction in τ_0 and increasing P_H (contact pressure) as predicted in Eq. 2.1. However, the CoF is not an intrinsic (material) property as it is variant under different conditions (i.e. independent of

load, sliding speed, contact area, and other operational variable) [1]. Figure 2.2 shows the variability of the frictional properties for common lubricants and other materials.

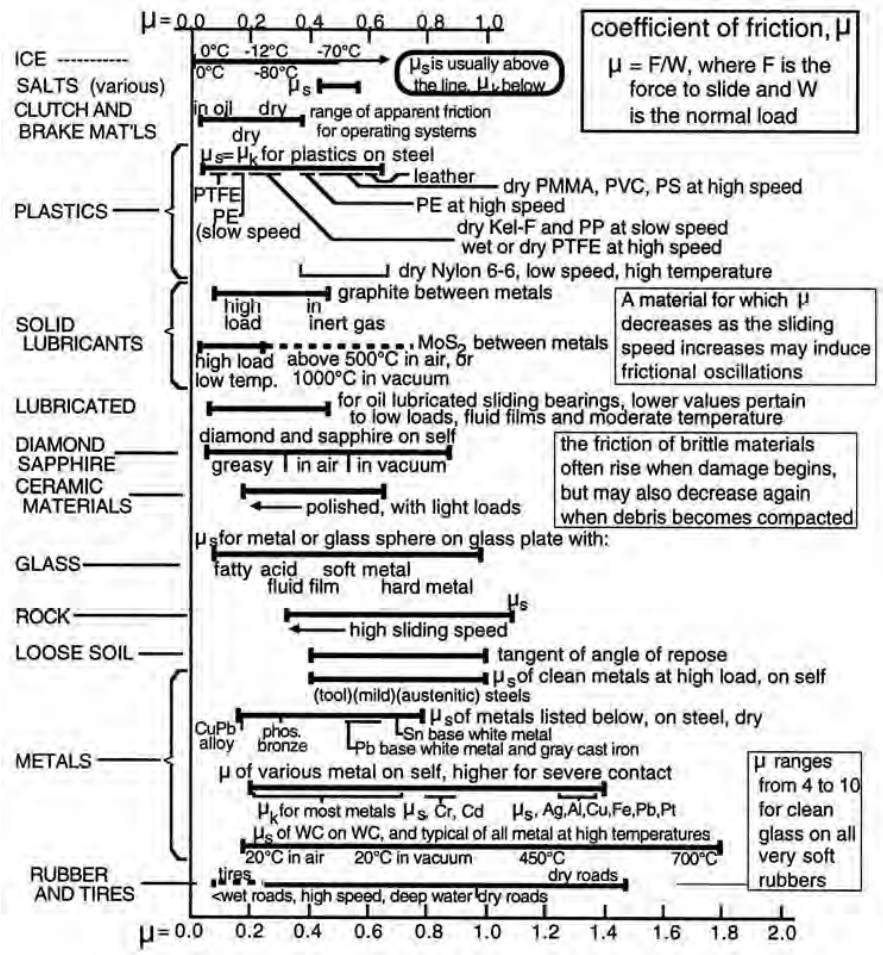

Figure 2.2: A diagram of the coefficient of friction based on various metals and conditions of sliding. [1]

For example, MoS_2 in contact with metals is shown to vary from 0.01 to 0.7 as the temperature increases along with showing a dependence to humidity. Even so, friction is generally regular and steady during relatively constant sliding conditions. However, based on the conditions at the initial break-in period, changes in friction occur due to the mixing and formation of new surfaces. In air, for example, the surfaces (contacting bodies) and their corresponding debris will likely oxidize, while sliding contact pressures at the interface induce the formation of tribolayers in between the contacting bodies [1-5] which can be passive after their formation. Both the static (normal) and

dynamic (sliding) contact stresses contributes to the overall friction behavior experienced by the contacting bodies, but the dynamic sliding stress fields ahead of the counterface are compressive and behind are tensile, which increase the maximum subsurface shear stress compared to static.

Figure 2.3 shows the common factors that induce frictional forces. Bowden and Tabor (1950) classically explained friction as the asperities from different surfaces coming into contact and welding together due to adhesion (Fig. 2.3(a)). They also include the concept of ploughing. This occurs when hard asperities and/or wear particles are trapped at the sliding interface and plough through the surface by plastic deformation of the softer surface, which causes resistance in the sliding direction (Fig. 2.3(b)).

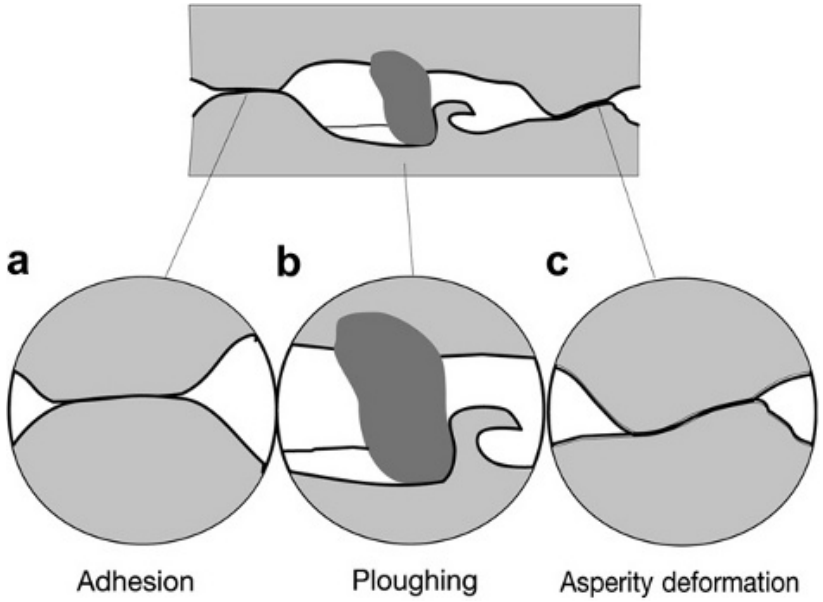

Figure 2.3: Common mechanisms for frictional resistance during sliding of contacting bodies. [3]

In addition, a component for plastic deformation of asperities during sliding was further introduced. It's apparent that asperity interactions play a prominent role in the friction behavior, microscopically. As seen in Fig. 2.3 and 2.4, contacting surfaces are rough (i.e. not perfectly flat), and the real area (Ar) is orders of magnitudes (10^{-2}-10^{-6}) smaller than the apparent area (A_a). Based on this, the apparent area should be as low as possible to minimize adhesion as the asperities can

still experience plastic deformation over elastic stresses, where the bulk does not, due to localized stresses that exceed the elastic limit of the tip of asperities [4].

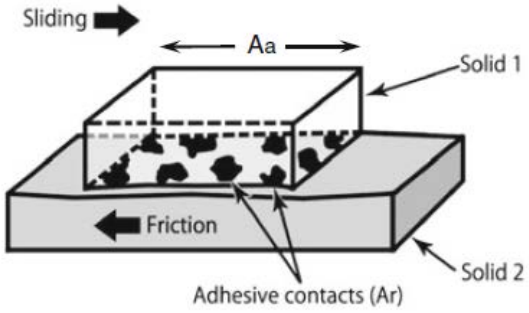

Figure 2.4: The apparent area of contact compared to the real (asperity) area of contact during dry sliding of contacting bodies. [4]

Greenwood and Williamson developed a theory which modeled the changeover from elastic to plastic contact for rough contacting surfaces under static loads with the assumption that the asperities are spherical and follow a Gaussian distribution [1,3-4]. They calculated the plasticity index (ψ) as:

$$\Psi=\frac{E^*}{H}\sqrt{\frac{\sigma_S}{R_S}} \quad (2.2)$$

where the reduced Young's modules E* is

$$\frac{1}{E^*}=\frac{1-\upsilon_1^2}{E_1}+\frac{1-\upsilon_2^2}{E_2} \quad (2.3)$$

where $E_{1,2}$ and $\upsilon_{1,2}$ are the elastic modulus and Poisson's ratio of contacting materials 1 and 2, respectively, H is the hardness of softer material, σS is the standard deviation peak, and R_S is the composite peak radius. The plasticity index, a non-dimensional value, predicts that when $\Psi<0.61$ elastic deformation dominates, while $\Psi>1$ will involve predominantly plastic deformation [3,4]. Furthermore, the A_r can be estimated for elastic contacts and was determined to be proportional to the normal load and inversely proportional H. Thus, it indicates that the adhesive forces can be minimized by lowering the A_r and increasing the H and E.

2.1.2 Dry Sliding Wear

For most applications, specifically moving mechanical assemblies, energy-reducing and wear resistant materials/coatings remain as the over-arching features focused on during the design process of any industrial component. Wear, specifically dry sliding, is a degradation process in which one or both surfaces in relative motion are elastically or plastically deformed, and characterized by loss of material from a surface and/or transfer of material from one surface to another [2]. Figure 2.5 shows the different wear mechanisms and their corresponding wear coefficient range where lubricated contacts are on the order of 10^{-5}-10^{-14} ($mm^3/N \cdot m$). Solid lubricants will generally experience boundary, mild, abrasive and/or corrosive wear whereas liquid lubricants operate in the hydrodynamic lubrication, elastohydrodnamic lubrication and boundary region. Therefore, liquid lubricants will generally prevent less wear to components in many conditions, but as already mentioned they are not effective at high temperatures and extreme contact pressures where solid lubricants are more applicable. The wear coefficient K is defined as the product of specific wear rate, which is the wear volume per unit distance and load, and hardness of the wearing material [1-2]. Either term (specific wear rate or K) can be used to define the relative amount of wear.

Similar to friction, wear is a system response that is affected by normal load, sliding velocity, environment, and temperature, and exhibits several different wear mechanisms to accommodate changes in conditions. A wear mechanism defines the process of material removal from the contact surface, and depends on the contact conditions [2,6]. The main wear mechanisms for dry sliding surfaces are: (i) abrasive wear (hard surface against soft); (ii) adhesive (material transfer and removal); (iii) fatigue wear (cyclic crack growth and delamination); and (iv) chemical wear (corrosive, tribochemistry, oxidative, etc.) [2-3,7].

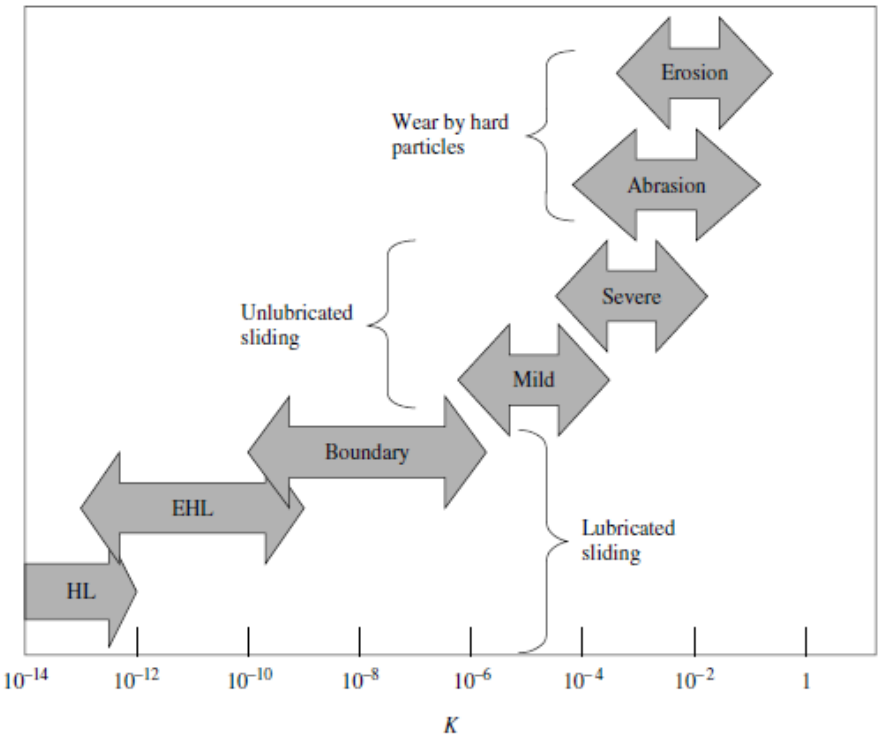

Figure 2.5: Representation of the range of wear coefficient K under different lubrication conditions. [2]

Abrasive wear and asperity deformation occurs when a considerably harder asperity or wear (debris) particle are dragged through a softer surface, which is characterized by grooves (microcutting) and scratches due to plastic flow (ploughing) of the softer material. Adhesive wear occurs when asperities come into contact, weld together and remove material from the softer surface, which is important to understand for failure modes such as scuffing and seizure [3]. Fatigue wear is defined as crack growth from loading and unloading of a surface, resulting in large-scale cracking and liberation of surface material through delamination of wear plates (tribolayers) or the formation of wear debris. Chemical wear occurs by detrimental (sometimes not) chemical reactions at the surface due to the mechanical stresses and environmental conditions (e.g. high/low temperature, dry/ambient air, etc.) where oxidative wear is the most common process. Velocity accommodation is another concept that can also be used to explain wear mechanisms and their

classifications, which is accounted for in Eq. 2.1 with τ_0. The difference between two surfaces in relative motion can be accommodated, generally, by elastic deformation, fracture, shear and rolling [3] at the interfaces, which can occur by two surfaces (first bodies) or in the tribolayer at the interface (third body) [2-3,7]. There have also been several other velocity accommodation mechanisms that have been postulated [9].

In addition to wear mechanisms, there are wear modes which classify the specific types of contact (e.g. movement, geometry, environment, etc.). Sliding wear by microcutting, fatigue by crack initiation, corrosion by delamination, and impact wear are examples of wear modes, while scuffing, pitting, scoring, spalling, etc., are examples of wear failure modes [2-3]. Shown is Fig. 2.6 is the characteristic wear modes exhibited by the different wear mechanisms. Based on the conditions, moving mechanical assemblies will undergo one or more of these wear modes during dry sliding due to the materials behavior and reactions.

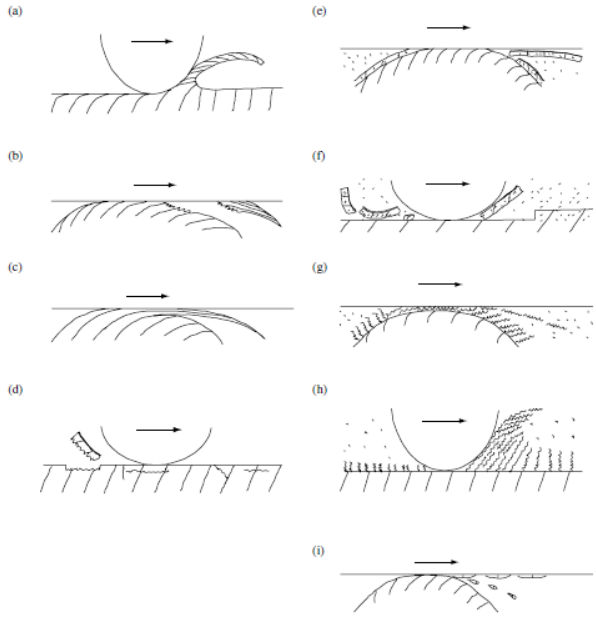

Figure 2.6: Different wear modes: (a) abrasive wear by microcutting; (b) adhesive wear from shear and transfer; (c) flow wear by accumulated plastic shear flow; (d) fatigue wear by crack propagation; (e) corrosive wear by shear fracture of ductile tribofilm; (f) corrosive wear by delamination of brittle tribofilm; (g) corrosive wear by accumulated plastic shear flow; (h) corrosive wear by shaving; and (i) melt wear. [2]

2.2 Solid Lubricants

Within the last 50 years, advanced solid lubricant materials and coatings have become an important area of research for mechanical and engineered systems, which provide low friction and high wear resistance, and rely on high performance, durability and efficiency [1]. By a velocity accommodation, oils and grease act to reduce the friction between sliding surfaces through the oil molecules shearing across the sliding interface to form a protective film at the interface [7]. At elevated temperatures (>350°C), oils generally fail (depending on their grade) due to volatilization and/or chemical reactions that lead to early failure of lubricated components, while at lower temperatures (cryogenic) oils will solidify or congeal preventing lubrication. Furthermore, oils and greases tend to volatilize during exposure to high vacuum or inert atmospheres. Therefore, solid lubricants are used in low (cryogenic) and high temperature (>500°C) where oils are inadequate.

2.2.1 Coating Classification

Solid lubricants are classified as either intrinsic or extrinsic where intrinsic lubricants possess an atomic structure that facilitates low interfacial shear stress (e.g. MoS_2 and graphite), while extrinsic lubricants require an additive (e.g. second phase) to promote low interfacial sliding stress and/or load-bearing surfaces [7]. Similar to oils, intrinsic and extrinsic lubricants oxidize at the higher temperature causing destructive abrasive wear, but some soft metals (e.g. Ag, Au, Cu, etc.), fluorides (e.g. CaF_2), and metal oxides (e.g. V_2O_5, NiO, WO_3, etc.) at elevated temperatures have been shown to plastically deform and form low-shear-strength surfaces [7]. At relatively low temperatures, however, these phases are generally not lubricious. Thus, chameleon coating were developed with the goal of developing an adaptive surface during thermal cycling from RT to 1000°C that maintains low friction and wear [17-18]. An example of a chameleon coating is the

PS (Ni-Cr system) coatings developed by NASA. The CoF was maintained between 0.2-0.3 from 25°C to 850°C by adding Ag for low/moderate temperatures lubrication and alkali fluorides for high temperatures lubrication, which provides low friction at all ranges due to a synergistic effect between lubricants [18]. In addition, coatings can be classified as soft or hard. Soft coatings, when sliding against a hard surface, form a thin soft surface layer by plastic deformation that can partly transfer by adhesion. The transfer layer is displaced into the sliding interface and provides easy facilitation of shear (i.e. low shear strength), which lowers the COF and wear [15]. Conversely, hard coatings act as a load-bearing element that lower the area of contact, preventing plastic deformation and thus lower fiction and wear. By integrating these types of coatings (i.e. soft matrix embedded with a hard phase), the tribological properties, specifically wear resistance, can be drastically improved based on previous studies [13,15, 22-27]

2.2.2 Ni-base Metal Matrix Composites

Nickel and Nickel base superalloys are used for component in aerospace and structural applications due to their high strength and resistance to oxidation at high temperatures. Emergent research in MMCs reinforced with ceramic particles (e.g. oxides, carbides, nitrides, etc.) aims to improve the wear resistance of such coatings for use in dry sliding applications, while avoiding formation of abrasive compounds, such as Al_2O_3, W_2C, and Ni_2W_4C, which can adversely affect their tribological properties [13-14,21-27]. The addition of hard particles also improves coating cohesion efficiency by creating micro-asperities that promote bonding, lowering porosity and increasing density of the cold sprayed coatings [10,13-15]. MMCs coatings are a major focus of tribological research due to their attractive mechanical, thermal and chemical properties, which conventional metals and alloys do not provide [10], for heat engines, high-speed bearings, high

temperature seals, etc. [11]. WC particles are common reinforcing particles in MMCs due to their high hardness, strength, and fracture toughness compared to other carbides/oxides. They are often used in a combination with Ni as a metallic binder, and thus Ni-WC composites have been shown to be effective at reducing wear [22-27]. Van Acker et al. [24] studied the effect of WC particle size and volume fraction on the sliding wear behavior of laser clad Ni-WC coatings. The wear rate was found to decrease logarithmically with the addition of WC up to a volume fraction of 50%. Surender et al. [40] showed that increasing the WC content from 10 to 37 vol. % caused a reduction of friction coefficient from ~0.5 to 0.35 due to an increase in surface hardness and reduction of the plastic deformation contribution to the friction coefficient. However, Xu et al. [25] determined that the addition of above 27 vol. % WC in the powder feedstock led to an increase in the wear of laser cladded WC/Ni coatings and facilitated a transition from two-body abrasive to third-body abrasive and surface fatigue wear. Based on these studies, there is an optimum volume fraction of WC particles of around 30 vol. % in Ni matrix to produce reduced wear coupled with low friction coefficient

Previous studies on the dry sliding properties of nickel-based coatings at room temperature revealed the formation of mechanically mixed layers (MML) by compaction of nanocrystalline oxides particles at the sliding interface that resulted in decreasing friction and wear [27-29]. Fernández et al. [26] studied the sliding wear of a laser cladded NiCrBSi alloy reinforced with WC particles and found that the wear resistance of the reinforced coating improved due to a formation of a compacted oxide layer on the contact surface which had reduced adhesive wear. While, Alidokht et al. [27] showed that the room temperature wear rate of a cold sprayed Ni-10.5 vol% WC coating was significantly lower compared to a cold sprayed pure nickel coating. Furthermore,

they determined that WC particles promoted the formation of a stable MML composed of nanocrystalline/amorphous oxygen-rich nickel.

2.2.3 High Temperature Lubricious Oxides

As mentioned there are several applications that require solid lubricants for HT applications (above 350 °C) such as air foil bearings and high speed machine tools. One potential candidate is binary and ternary oxide coatings that form lubricious phases above 300°C. Due to the structural and chemical (i.e. thermodynamics) stability of oxides at higher temperatures, these phases are being investigated for tribological applications for lubrication purposes at elevated temperatures which take advantage of oxidative exposure. There are five mechanisms associated with enhanced mechanical and tribological performance observed for binary and ternary oxides. These mechanisms [7] are: (i) easy shearing due to screening of cations by surrounding anion (crystal chemical model); (ii) material softening corresponding to a brittle-to-ductile transition of most oxides; (iii) melted oxide (i.e. above Tm, similar to liquid lubrication); (iv) weak inter-planar cohesive bonds (graphite and MoS2); and (v) shearing in textured nanocrystalline grains due to dislocation glide (intracrystalline slip).

For nickel and nickel alloys at elevated temperatures, they readily form a compacted oxide layer, also termed a glaze layer that reduces friction in dry sliding contact [29-32]. This glaze was determined to consist of 10-50 nm NiO particles that were compacted from the induced pressure and localized flash temperatures that occurred during dry sliding [28-31]. Furthermore, the glaze was found to form at the contact area because of sliding-induced flash temperatures and oxidative wear [30, 33-35]. The formation and growth of nickel oxide glaze layers has been studied by Jiang et al. [31] while studying a nickel-based alloy under dry sliding conditions up to 250°C. A

conceptual model was proposed describing the tribo-mechanics of the compacted oxide debris, which they characterized as tribo-sintering of entrapped wear debris particles in the sliding contact area. A lubricious and wear-resistant oxide layer subsequently forms due to fracture and sintering under highly localized pressure and temperature. This complex phenomenon was observed at different temperatures and pressures depending on the material system [30-31,34]. Furthermore, Hager et al. [32] investigated the tribological properties of cold sprayed pure nickel coatings against Ti-6Al-4V alloy. They concluded that the formation of a NiO transfer film, which was more prominent with higher operating temperatures, resulted in a reduction in friction coefficient. Under these conditions, work-hardened wear debris particles were more readily compacted and sintered together.

2.3 Cold Spray

2.3.1 Principles of Cold Spray

CS processing exploits solid state deposition of solid particles (ca. 40 μm diameter), which is enabled by accelerating particles to velocities between 400 and 1200 m/s (see Fig. 2.7). The particles acquire sufficient kinetic energy to undergo plastic deformation and adhere to the surface [10-11,16]. If a critical velocity is achieved upon impact, the particles are thought to undergo adiabatic shear instability [10-11], which causes subsequent plastic deformation from thermal softening and adherence to the substrate. The resulting strong particle/substrate and particle/particle cohesion leads to the formation of a strongly adherent coating. In cold spray, particles remain in solid state due to the short contact time with the high-temperature carrier gas, and the gas temperature is lower than the melting points of the particles. This helps to avoid high

temperature induced effects such as residual tensile stress, oxidation or phase changes that could be detrimental to the coating's tribological performance.

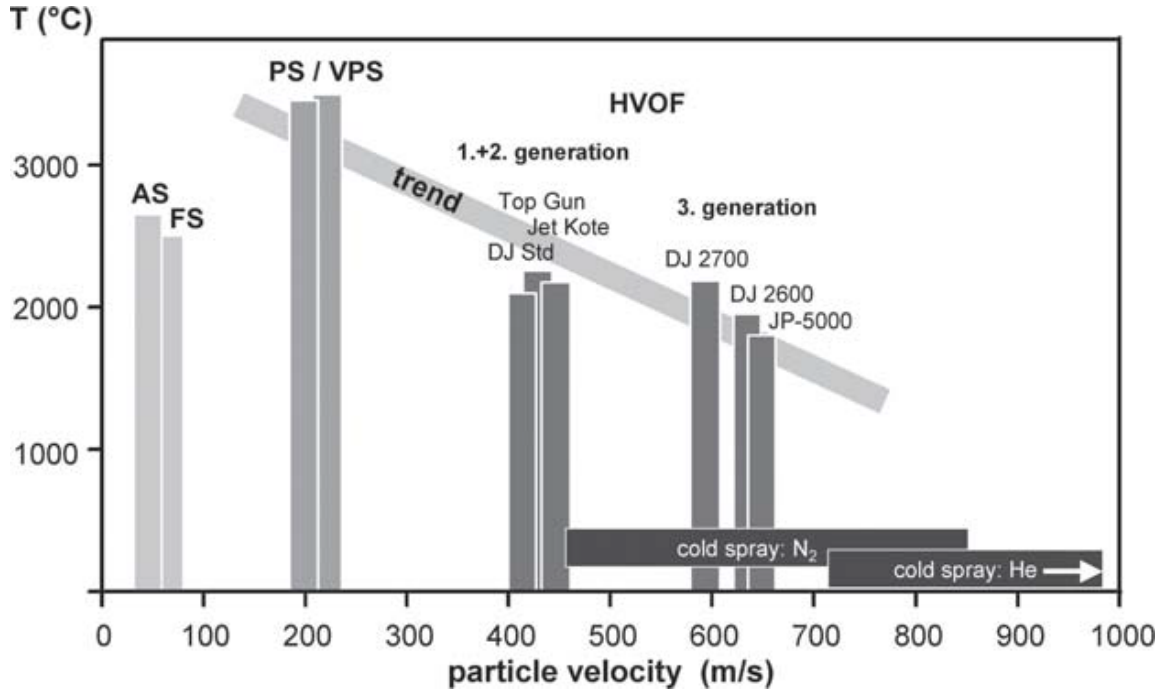

Figure 2.7: Particle temperatures and velocities of cold spray compared to other common thermal spray processes. [16]

Whereas, these effects are prevalent in laser cladding and plasma spray processes due to their higher processing temperatures [23-25]. Figure 2.7 shows the particle temperature in relation to the particle velocity where high velocity oxy flame (HVOF) and plasmas spray easily surpass 1500°C and 3000°C, respectively. At these temperatures, particles will undergo melting, dissociation and/or phase transformation that adversely affect the tribological properties, causing unexpected failures. Overall, the CS process relies on choosing the optimal particle velocity that is between the critical velocity (good adhesion) and erosion velocity (erosion occurs instead of adhesion) to form a dense and compact coating.

2.3.2 Advantages and Limitations of Cold Spray

Due to the unique techniques provided by cold spray and the subsequent properties, it is an applicant for developing novel coatings. Cold sprayed coatings are shown to provide excellent wear resistance for parts in sliding, rolling, and fretting contacts, thereby improving the engineering lifespan of various components, especially those found in the automotive and aerospace industries [12,14-16]. As mentioned above, cold spray processing exploits comparatively low processing temperatures during deposition. The low processing temperatures allow for high deposition rates and residual compressive surface stresses to be stored, while avoiding residual tensile stresses, oxidation and phase changes which are often detrimental to the coating tribological performance. Furthermore, thick coatings (5-500 microns) can be obtained through this technique with the benefit of precise control on the area of deposition [16]. The cold spray processing approaches are also beneficial for the synthesis of multicomponent or composite systems, opening avenues to engineer environmentally self-adaptive tribological systems, following general concepts reported earlier [17-20], and provide considerably higher growth rates and resulting coating thicknesses when compared to physical vapor deposition methods used in these reports. There are a few drawbacks to CS. High pressure powder feeders are sometimes required for cold spray, which can lead to nozzle clogging, especially at higher temperatures and velocities, and nozzle wear due to particle erosion [16].

2.3.3 Cold Spray of Metal Matrix Composites

To facilitate the deposition of brittle materials, MMCs were theorized due to the ductile properties of metals. With the low processing temperatures, cold spray prevents unwanted chemical reactions between the metal and ceramic powders, allowing for high density and low

porosity coatings, which is why CS is a favorable technique for processing MMCs. The tribological properties of cold sprayed MMCs can be fine-tuned by adjusting several processing parameters such as gas temperature, particle velocity, substrate material, etc., and more importantly, by controlling the amount of wear resistant ceramic particles that are retained into the coatings [14]. The secondary hard particles are also shown to remove oxide layers, contaminations and impurities, while improving bonding due to the formation of microasperities [16]. However, because of the low processing temperatures, there can be an issue of secondary phase retention, which is generally addressed by increasing the gas temperature or adjusting the feed rate [27,39].

CHAPTER 3

MATERIALS AND EXPERIMENTAL PROCEDURES

3.1 Fabrication of Coatings

Mild steel plates, 3 mm thick, with a hardness of 175 HV were used as substrates. Plates were cleaned in acetone and then grit blasted prior to deposition. Commercial pure water atomized Ni (AMPERIT® 176, H.C. Starck, Munich, Germany) and agglomerated and sintered WC/Ni (AMPERIT® 547, H.C. Starck, Munich, Germany) were used as feedstock powders. The cold spray process was conducted using a PCS1000 system (Plasma Giken, Japan) with nitrogen as the carrier gas. Prior to entering the de Laval nozzle the gas pressure was 4 MPa and temperature was 800°C. The stand-off distance between the substrate and nozzle exit was set to 40 cm and the gun traverse speed was fixed to 30 mm/s. The particle velocities were measured in a free-jet by a time-of-flight particle diagnostic system. A mixture of Ni-36 vol. % WC (Ni-45 vol. % WC/Ni) was sprayed (see table 3.1). The co-feeding system was used to avoid problems arising from difficulty in admixing powder of differing densities and/or damage to powders due to mechanical mixing. The as-sprayed Ni and Ni-WC coatings were 1.9±0.7 and 1.53±0.05 mm thick, respectively.

Table 3.1: Cold spray deposition characteristics of the powders.

Powders	Volumetric feeding rate (cm3/min)	Mass feeding rate (g/min)	Volume (vol. %)	Powder in the initial feedstock (wt. %)	Apparent density of powders (g/cm3)
Ni	6	21	55	50	3.5
WC/Ni	4.8	22	45	50	4.5

3.2 Cold Spray Deposition

3.2.1 Instrument Parts

The cold spray process was conducted using a PCS1000 system (Plasma Giken, Japan). The processing set up is shown in Fig. 3.1 where two separate hoppers feed the Ni and WC/Ni powder into pressurized carrier gas that was forced out a de Laval nozzle. Nitrogen was used as the carrier. Prior to entering the nozzle the gas pressure was 4 MPa and temperature was 800°C. The stand-off distance between the substrate and nozzle exit was set to 40 cm and the gun traverse speed was fixed to 30 mm/s.

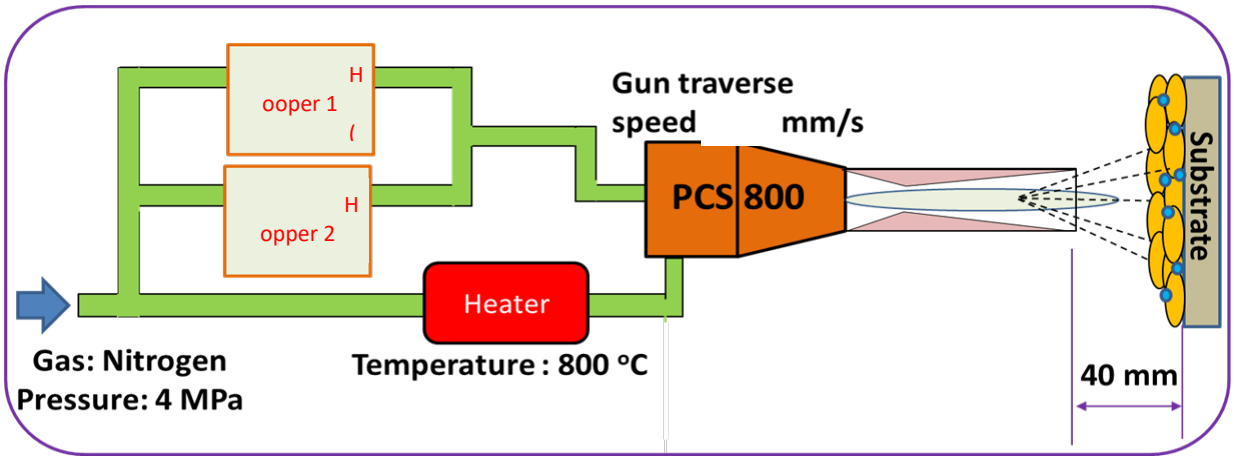

Figure 3.1: Schematic of cold spray configuration

3.2.2 Powder Description and Powder Feeder

Laser particle size analysis (LA-920, Horiba, Kyoto, Japan) was used to measure feedstock powder size distribution. The Ni and WC/Ni powders had particle size ranges of -35+15 µm (d50=25 µm) and -30+5 µm (d50=23 µm), respectively. Figure 3.2 shows a SEM image of a WC/Ni agglomerate along with corresponding elemental EDS maps. The brighter contrast phase corresponds to agglomerated WC particles, the lighter (grey) contrast phase is Ni, and the dark contrast phase correlates to free C which was added to eliminate remaining porosity. Based on the supplier data sheet, C content is 5.4-5.8 wt. %. Considering that C is primarily in the WC

compound (5.4 wt. %), there should be less than 0.4 wt. % (0-2.5 vol. %) of free carbon. The WC/Ni (WC-20 vol. % Ni) and Ni powders were fed to the gun from separate hoppers and, by setting feed rates, a mixture of Ni-36 vol. % WC (Ni-45 vol. % WC/Ni) was sprayed (see table 3.1). The particle velocities were measured in free-jet by a time-of-flight particle diagnostic system (ColdSprayMeter, Tecnar, Canada). The velocities of Ni and WC/Ni particles at the given spray conditions were determined as 659±125 and 569±108 m/s, respectively.

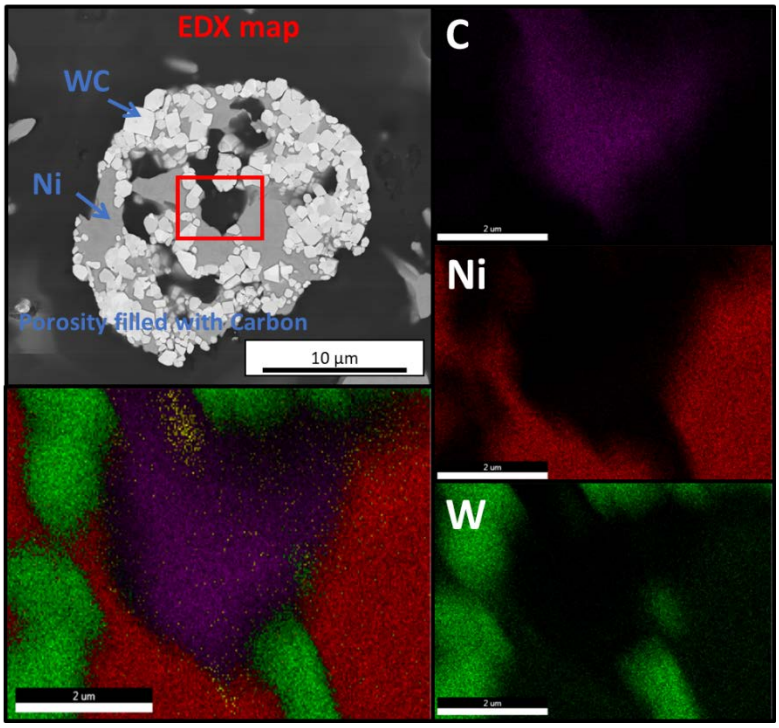

Figure 3.2: Elemental EDX maps of WC/Ni powder

3.2.3 Sample Preparation

To remove the cold sprayed samples, a Mitsubishi FX 10 wire EDM was used. By sending a high current through the brass wire, an electric field is created between the wire and sample, which is submerged in a dielectric field. Due to this process, the wire cuts through the material at fine precisions. Cold sprayed coatings were cross-sectioned perpendicular to the gun traverse direction, mechanically ground, polished using 9 µm, 3 µm, and 1 µm diamond suspension, and

finished by polishing with 0.05 μm colloidal silica. Once polished, the samples were placed in ethanol, and then put into the sonicator for 10 minutes to remove any nascent impurities left on the surface from polishing.

3.3 Coating Characterization

3.3.1 Vickers Micro-Hardness Testing

The indentation hardness of the coatings at room and elevated temperatures were measured ex situ with a Vicker's microhardness tester (Tukon1102- Wilson Hardness) by applying a normal load of 10 N (HV1) for a 10 second hold time. Areas of indentions were selected randomly, with at least 10 indents per sample, to determine average hardness values.

3.3.2 Scanning Electron Microscopy (SEM)

SEM was used to characterize the microstructure and composition (through EDS) of the (un)worn surface to better understand the wear mechanism during dry sliding. A FEI Quanta 200 ESEM with a W filament capable of 3 nm resolution was used to image the worn surface, while an equipped EDAX EDS (Sapphire Si(Li) detecting unit) system was used for phase identification.

3.3.3 X-Ray Diffraction (XRD)

A Rigaku Ultima III x-ray diffractometer was used to identify crystallographic phase of the as-deposited Ni and Ni-WC at room temperature. Cu Kα incident x-rays (λ=0.154 nm) were generated at a source of 40 kV and 44 mA. The parameters used were a 0.01 step size and 1°/min scan speed from 20° to 90° (2θ value). Jade v10 software was used to analyses the XRD peaks.

3.3.4 Raman Spectroscopy

A Nicolet Almega XR Dispersive Raman spectrometer with a 532 nm (green) laser was used to determine the phases present on the surface of the worn regions. Omnic™ analytical-software was used to collect and manipulate the collected Raman spectrums.

3.3.5 Optical Microscope

Optical imaging of the as-deposited coatings and WC-Co counterfaces were taken to understand the induced effects of temperature of the sliding surfaces (i.e. wear on the surface). A Zeiss Axio Lab. A1 with an objective range of 5-100x magnification was used.

3.3.6 Interferometer

White light interferometry (Rtec) measurements using a 10x Nikon interferometric objective lens were done to determine the volumetric loss of material by wear from the scanned profile. Gwyddion, an open source software, was used to analysis the profiles and obtain a volumetric loss. The wear volume was then divided over the normal load (2.5 N) and sliding distance (200 m) to obtain specific wear rates in $mm^3/N \cdot m$ units.

3.4 Tribological Testing

3.4.1 Pin on Disk Tribometer

Sliding wear tests were conducted using a Falex ISC-450 unidirectional pin-on-disk (POD) tribometer. Figure 3.3 shows an image of the high temperature tribometer along with a schematic representing the POD configuration. Hard WC-Co balls (1500 HV) with a diameter of 6.35 mm were selected as the counterface material to minimize ball wear. All tests were performed using a

sliding velocity of 2 cm/s, a sliding distance of 200 m, and a normal load of 2.5 N, correlating to a 1.1 GPa and 1.4 GPa maximum Hertzian contact stress for pure Ni and Ni-30 vol% WC, respectively. In addition, sliding wear tests were run in open air with a relative humidity of ~40%. A heating coil under the stage and two heat shields enclosing the tribometer enabled testing at elevated temperatures (see Fig. 3.3), which was set at 200°C or 400°C. At least three tests were performed for each coating at each temperature. Thermal cycling tests were also conducted by repeated placement and removal of the heat shields during sliding after a set distance to either increase or decrease the temperature, respectively.

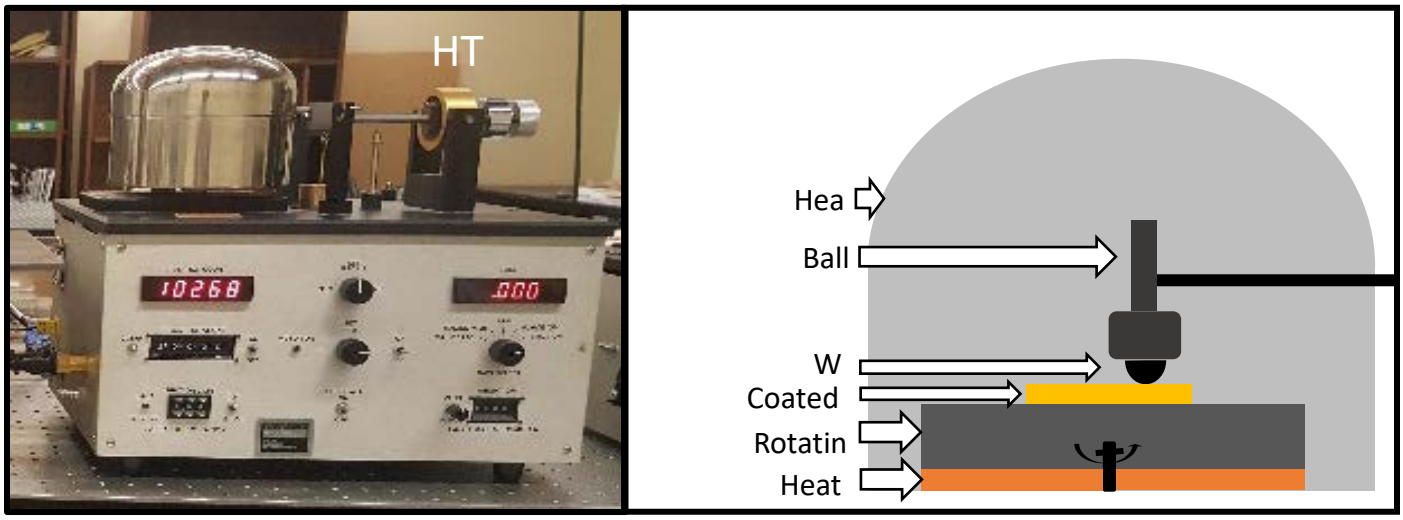

Figure 3.3: Image of the high temperature tribometer set up and diagram of the pin-on-ball configuration inside the heating shield.

CHAPTER 4

DRY SLIDING WEAR BEHAVIOR AND MECHANISMS OF COLD-SPRAYED Ni-WC COATINGS AGAINST WC*

4.1 Coating Structure

The room and elevated temperature microstructure and hardness of the as-deposited Ni and Ni-WC coatings were evaluated with XRD, Raman spectroscopy, and microhardness testing. XRD scans (not shown) for the pure Ni coatings displayed the characteristic diffraction peaks of FCC nickel. Oxide peaks were not observed due to the low processing temperatures associated with the cold spray [12,14]. However, EDS of the as-deposited coating surface (see Table 4.1) detected the presence of less than 1 wt. % O on the surface due to the formation of a thin native oxide layer at the surface.

Table 4.1: Elemental composition of the as-deposited Ni-WC coating with standard deviations.

Element	Wt. %	At. %
Ni	72 ± 2.2	70 ± 1.0
W	23 ± 2.4	7.0 ± 1.0
C	4.6 ± 0.2	22 ± 0.7
O	0.5 ± 0.4	1.7 ± 1.2

Figure 4.1 shows the XRD scan for the cold sprayed as-deposited Ni-WC coating. Observed diffraction peaks correspond to FCC Ni and hexagonal WC (P-6m2 space group) phases. After deposition, no new phases were revealed, such as W_2C or other intermetallic carbide phases, which are typically found in the microstructure of WC/Ni coatings processed at higher temperatures (e.g. laser cladding) [23-25]. Around 80% of WC/Ni particles were recovered in the

*Content from this chapter is reproduced from T.B. Torgerson et al., "Room and Elevated Temperature Sliding Wear Behavior of Cold Sprayed Ni-WC Composite Coatings," Surface Coatings and Technology, (in press), with permission from Elsevier

coating, yielding a WC content of 30 vol. %. Image analysis through pixel count that was used to measure the WC content in the coating, showing a fill ratio of 30 vol. % WC for composite coating. This is close to the initial WC content in the feedstock, i.e. 36 vol. %. A previous study [27] found that a blend of Ni-36.2 vol. % WC, processed with a gas carrier temperature of 700°C, retained 10.5 vol. % WC in the cold sprayed coating. By increasing the carrier temperature to 800°C, the coating deposition efficiency increases drastically due to the higher particle velocities and a decrease in critical velocity by improving particle deformability [27]. WC/Ni particles retention mechanisms in various WC fill ratios was discussed in detail in an earlier work [39].

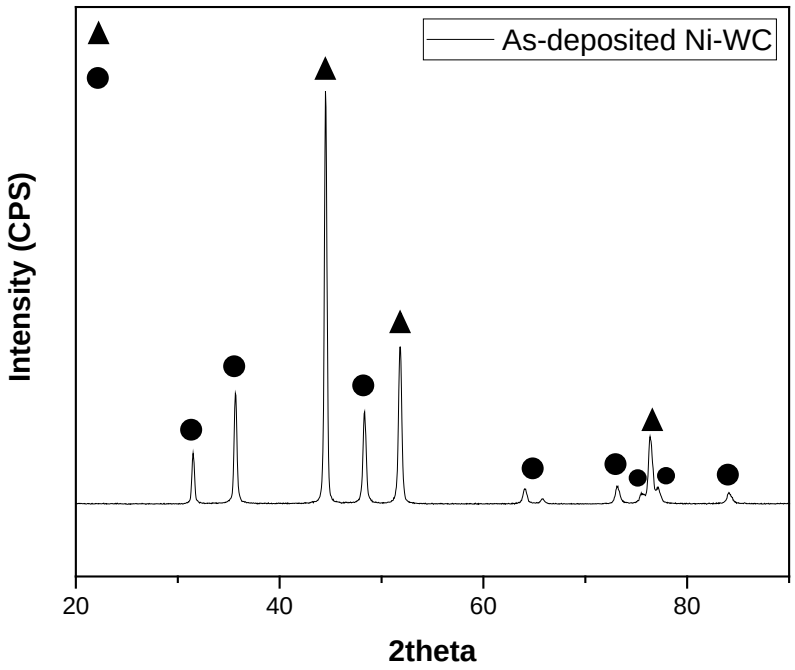

Figure 4.1: XRD scans of the as-deposited Ni-WC coating.

Table 4.2 lists the Vickers microhardness values measured at RT for pure Ni and Ni-WC coatings annealed at RT, 200°C and 400°C. The Ni coating exhibited an average hardness of 179 HV at RT, similar to previously reported values [32]. With the addition of WC to Ni, the microhardness increased to 264 HV at RT. This increase in microhardness is attributed to the harder WC particles in the Ni matrix. In addition, an increased density of the coating promotes a

harder surface as compared to pure nickel [25-27]. After heating the Ni-WC coating to 200°C, the microhardness of the annealed surface decreased to 235 HV.

Table 4.2: Microhardness values and standard deviations of Ni and Ni-WC coatings at RT, 200˚C, and 400˚C.

Coating	Hardness (HV)		
	RT	**200°C**	**400°C**
Ni	179±9	---	100±4
Ni-WC	264±17	235±12	160±13

This thermal softening is attributed to a release of the compressive stresses stored in the coating [13,32]. After heating to 400˚C, the microhardness of the annealed Ni and Ni-WC coatings decreased to 100 HV and 160 HV, respectively. This decrease in microhardness can be correlated to the further softening and annealing of the coatings forming larger grains that decrease shear strength and promote plastic deformation.

Figure 4.2 shows SEM images of the Ni-WC coating surface morphology at (a) RT and (b) 400°C. The darker contrast phase is the Ni matrix and the lighter contrast phase is WC. The roughness of the as deposited Ni-WC coatings (Ra=0.067 μm) had slightly increased to Ra=0.098 after heating to 400°C. Raman spectra (inset figures) were also collected at (a) RT and (b) 400˚C to identify the chemical phase compositions. No metal oxides were detected in the Raman spectra for the as-deposited coatings in agreement with the XRD scan shown in Fig. 4.1. However, according to the Raman spectrum shown in Fig. 4.2(a), there is a small amount of residual carbon detected inside some of the WC agglomerates. This phase (in black) is shown by the blue arrow in the SEM image in Fig. 4.2(a). XRD analysis (not shown) of the initial powders did not detect free-carbon, while EDS analysis of the cross section of powders and polished cold sprayed coatings

found the presence of free carbon. Figure 4.2(b) shows an SEM image and corresponding inset Raman spectra of the Ni-WC coating after annealing to 400˚C.

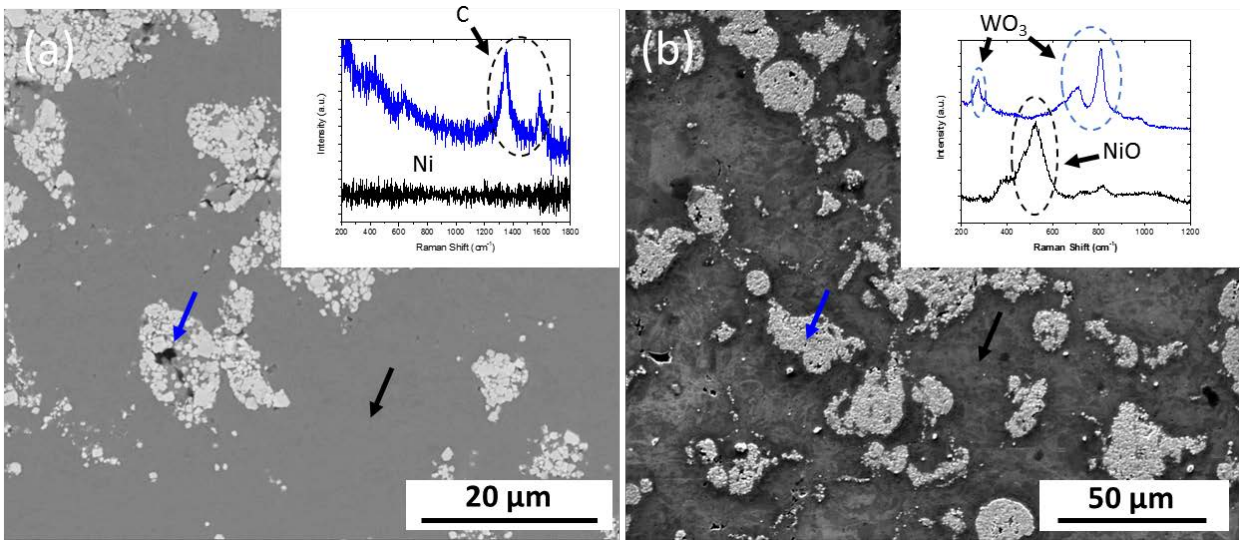

Figure 4.2: SEM images and inset Raman spectra of Ni-WC surfaces at (a) RT and (b) 400°C. Black and blue arrows denote the chemical phases in the Raman spectra.

Raman spectra indicate that the WC agglomerates oxidized due to the formation of WO_3 on the surface (lighter contrast region shown by the blue arrow in Fig. 4.2(b)), while the Ni matrix also oxidized to form surface NiO (darker contrast region shown by the black arrow in Fig. 4.2(b)). The surface chemistry of the Ni-WC coating after annealing to 200˚C (not shown) was similar to the RT Ni-WC coatings shown in Fig. 4.2(a). This suggests that the decreasing surface hardness from RT to 200°C is due to thermal softening of the coating, and the onset of bulk surface oxidation of these coatings occurs at a temperature between 200°C and 400°C.

4.2 Tribological Behavior

Typical sliding CoF curves of Ni and Ni-WC coatings tested at RT and 400°C are shown in Fig. 4.3. For RT testing, both coatings exhibited slightly lower CoF during the initial run-in period, for the first 15 to 25 m, before reaching a steady-state value of 0.41 and 0.50 for Ni-WC

and Ni coatings, respectively. The Ni-WC coating exhibited lower CoF values compared to the Ni coating due to the increased hardness of the Ni-WC, resulting in lower frictional contact caused by a reduction in the sliding contact area. Also, the elastic interaction of WC-Co with high modulus WC/Ni agglomerates, which increase the effective elastic modulus, act to reduce the CoF [40].

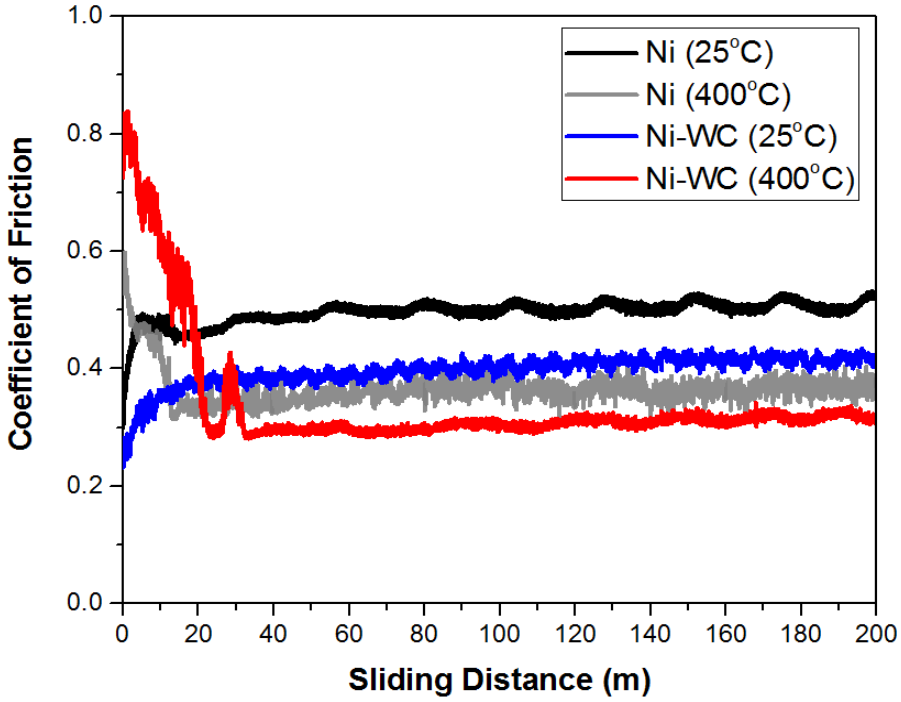

Figure 4.3: Representative coefficient of friction versus sliding distance at RT and 400°C of cold sprayed Ni and Ni-WC coatings.

Figure 4.3 also shows that during 400°C sliding both coatings exhibited decreasing CoF values upon reaching steady-state friction behavior after the first 15 to 20 m of sliding. The larger initial CoF values during the run-in period for both coatings is likely due to thermal softening, in agreement with decreasing hardness values listed in Table 4.2, which results in increasing sliding contact area and hence frictional contact. In addition, other studies have shown that CoF values were initially high due to the fracturing of the surface WO_3 and other oxide layers during run-in, and quickly reached low steady-state values as the wear debris was compacted into a uniform NiO

low-friction oxide layer [28-32]. This trend was previously reported in similar studies on Ni-based tribosystems [29-35]. It is evident that once lubricious oxides form on the wear surfaces low friction is achieved for both coatings with steady-state CoF values of 0.32 and 0.38 for Ni-WC and Ni coatings, respectively.

Table 4.3: Steady-state CoF and wear rate values with standard deviations of Ni and Ni-WC coatings at RT, 200°C, and 400°C.

Coating	CoF			Wear rate (×10-4 $mm^3/N·m$)		
	RT	200°C	400°C	RT	200°C	400°C
Ni	0.50±0.02	---	0.38±0.04	1.8±0.8	---	4.1±0.2
Ni-WC	0.41±0.03	0.59±0.05	0.32±0.02	0.5±0.4	7.3±1.2	3.7±0.4

The specific wear rates of the coatings were determined after 200 m sliding distance to further assess the tribological performance of the coatings. The wear rates of the Ni and Ni-WC coatings are listed in Table 4.3 along with their corresponding steady-state CoF values (taken from Fig. 4.3 friction curves) for the various testing temperatures. For RT sliding, the Ni and Ni-WC coatings exhibit wear rates of 1.8×10-4 $mm^3/N·m$ and 0.50x10-4 $mm^3/N·m$, respectively, which follows their reduced steady-state CoF values. As expected, the addition of the harder, load-bearing WC, particles improved wear resistance by preventing plastic deformation caused by adhesion at the mating interface and is in a good agreement with earlier reports [16-18]. However, for 400°C sliding, the wear rates increased to 4.1×10-4 $mm^3/N·m$ and 3.7×10-4 $mm^3/N·m$ for the Ni and Ni-WC coatings, respectively. This is in contrast to their decreasing CoF values during 400˚C sliding, which was likely aided by the aforementioned surface NiO layer formation, shown by the Raman spectra in Fig. 4.2(b). The identified opposite roles of thermal softening and the

formation of lubricious NiO tribolayers are critical for understanding and controlling Ni-WC MMC coating adaptive behavior at elevated temperatures.

To verify the competition between thermal softening and oxide layer formation, an intermediate testing temperature of 200°C was selected for the Ni-WC coating. Both the steady-state CoF (0.59) and wear rate (7.3x10-4 $mm^3/N \cdot m$) increased during 200°C sliding compared to RT testing. This indicates that thermal softening and the corresponding increase in sliding contact area were responsible for the increase in friction and wear, since, as mentioned above, Raman spectroscopy showed that the onset of surface oxidation occurs at a temperature greater than 200°C. Therefore, it can be inferred that if the low friction oxide layer did not form at 400°C, the coating's wear rate at 400°C would have increased to a higher value than the wear rate at 200°C. Instead, results indicate the eventual formation of the oxide layer mitigates further wear, as seen in Table 4.3. Thus, there is a time dependent competitive process between friction and wear during 400°C sliding, i.e., there was high initial friction and wear out to ~20 m of sliding that subsided with the eventual formation of the tribo-oxide layer. While not tested at 200°C, the cold sprayed Ni is expected to exhibit similar frictional behavior to the Ni and Ni-WC coatings at 400°C based on previous studies [28,32].

4.3 Solid Lubrication Mechanism of Ni-WC against WC

There is a clear distinction in wear mechanisms between the cold sprayed coatings as the temperature is elevated due to the formation of an oxide tribolayer at the sliding interface [27-30]. Figure 4.4 shows Raman spectra acquired inside the wear tracks on the Ni and Ni-WC coatings at RT and 400˚C. Figure 4.4(a) shows that for the Ni coating during RT sliding there is predominantly NiO present (~550 cm^{-1} Raman shift) on the wear surface with some mixed NiO and WO_3 detected

at increasing Raman shifts. Alidokht et al. [27] determined that a ~5 μm thick wear resistant mechanically mixed nanocrystalline/amorphous Ni layer rich in oxygen forms on the contacting surface of a cold sprayed Ni-WC coating.

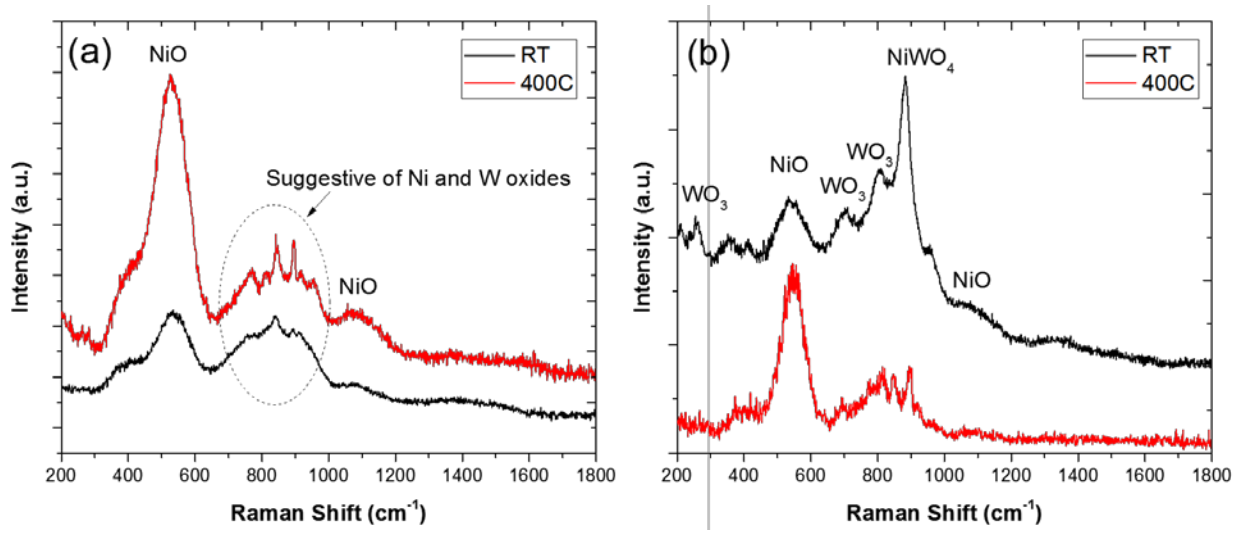

Figure 4.4: Raman spectra inside the wear tracks of (a) Ni and (b) Ni-WC coatings during RT and 400°C.

This explains the broad 550 cm^{-1} peak observed which is related to a defect structure, while crystalline NiO displays peaks at 460 and 500 cm^{-1} [37-38]. With elevated temperature sliding to 400°C, Fig. 4(a) shows that there is an increase in the intensity of the NiO peak at ~550 cm^{-1}, and thus the amount of NiO present on the wear surface. Therefore, this increasing amount of NiO phase is responsible for the decrease in CoF from 0.50 to 0.38 from RT to 400°C, respectively. Figure 4.4(b) shows that for the Ni-WC coating during RT sliding, in addition to NiO, there is also a clear presence of WO_3 and appearance of new tribochemical phase $NiWO_4$ at ~891 cm^{-1} Raman shift. This $NiWO_4$ phase was not present during static annealing, shown in the Raman spectra in Fig. 4.2(b), and thus it is a product of tribo-oxidation during RT sliding of Ni-WC coatings. This process involves oxidation of Ni matrix and WC debris to produce NiO and WO_3 accompanied by frictional forces that facilitate interfacial mixing to form $NiWO_4$, which remains stable at these

temperatures. Similar to 400°C sliding on the Ni coating, the Ni-WC coating in Fig. 4.4(b) shows that there is a dominant NiO phase present on the wear surface, while the WO_3 and $NiWO_4$ phases are considerably diminished. This confirms the aforementioned surface adaptive mechanism for friction reduction at 400°C is primarily due to the increasing amount of NiO phase forming a NiO-rich tribolayer, indicative of oxidative wear.

Figures 4.5(a) and 4.5(b) show low magnification SEM images of the RT wear tracks on the Ni and Ni-WC coatings, respectively. The Ni coating worn surfaces show plastic deformation and delamination characteristic of adhesive and surface fatigue wear. The white arrow in Fig. 4.5(c) revealed signs of adhesive wear whereby delamination occurred to generate wear platelets. According to EDS maps (Fig. 4.6), the delaminated surface layer shown in Fig. 4.5(c) is rich in oxygen indicating that the wear platelets are NiO, in agreement with Raman spectrum in Fig. 4.4(a), while underneath the platelets are predominantly Ni. In addition, the EDS map of W (see Fig. 4.6(c)) is overlapped with O suggesting WO_3 phase, which is also in agreement with the Raman spectra in Fig. 4.4(a). In previous studies, it has been determined that as Ni is plastically deformed during sliding, an unstable NiO layer forms on the coating surface that is compacted into an oxide glaze layer [26-29]. Furthermore, the interfacial shear stress from two-body adhesion caused tribolayer cracks, which results in the removal of protective oxides and subsequently exposing subsurface Ni to oxidation, then expanding and repeating in successive cycles.

In comparison, Fig. 4.5(b) shows that the Ni-WC wear track width is smaller than the Ni wear track width, corroborating with the decrease in the Ni-WC wear rate. In addition, the Ni-WC wear track exhibited less plastic deformation due to the WC phase. The higher magnification image of the Ni-WC wear track in Fig. 4.5(d) shows the presence of fine wear debris particles that resulted in some micro-abrasion. In addition, a distinct tribolayer in the middle of the Ni-WC wear track

formed, denoted by the white arrow in Fig. 4.5(d), which is elevated relative to its surrounding surface.

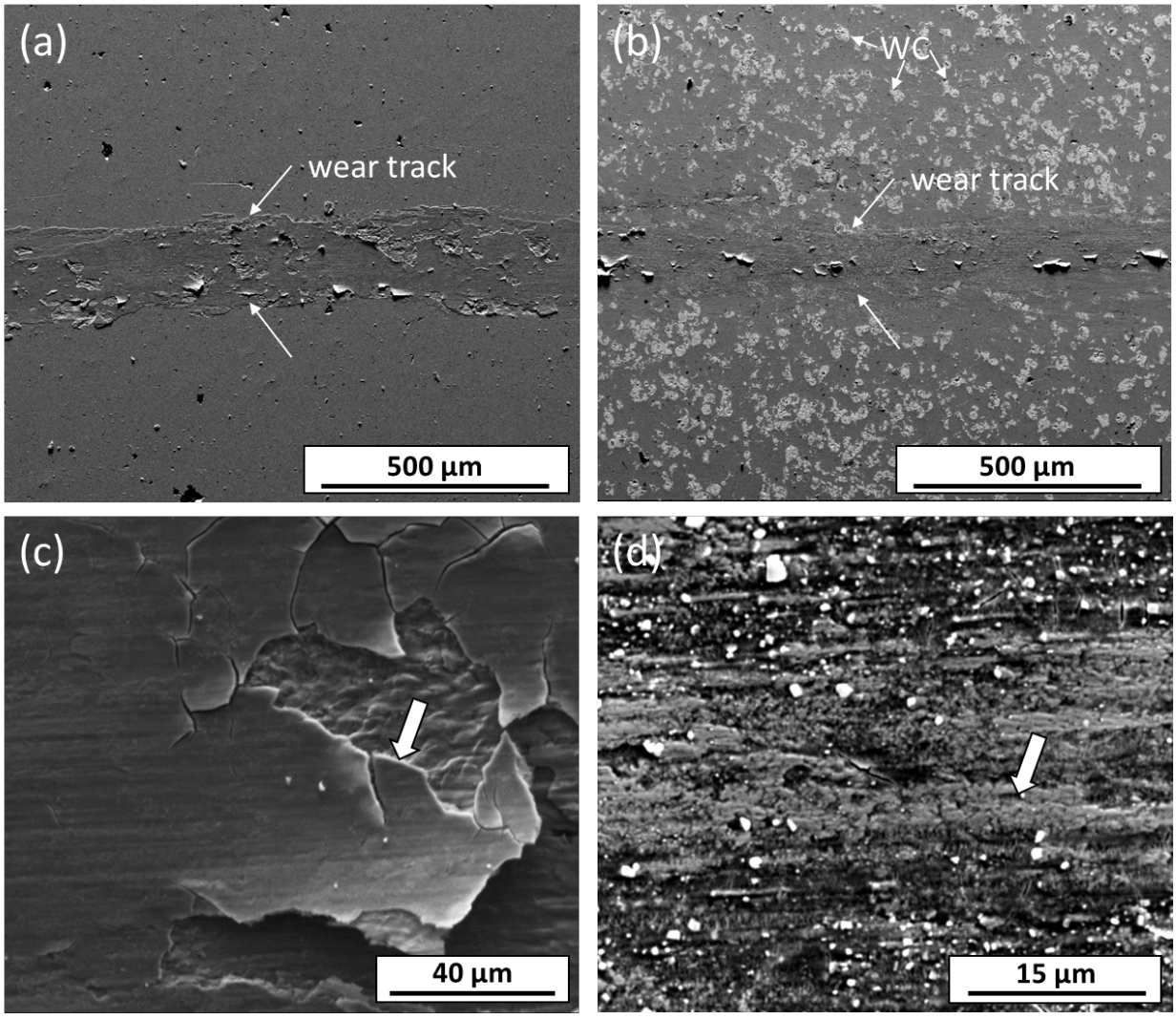

Figure 4.5: Low and higher magnification SEM wear track images on (a,c) Ni at RT and (b,d) Ni-WC at RT. White arrows in (c,d) show tribolayers.

Similar to the Ni coating, adhesive wear of the Ni-matrix occurred at the sliding interface along with the formation of NiO. Also, abrasive wear was present, indicated by the comminution of WC that recrystallized into oxide particles to form WO_3 debris, which is confirmed by the Raman spectrum in Fig. 4.4(b). As the counterface moved over this finer oxide debris, the compacted tribolayer was formed, which also contains the mechanically mixed $NiWO_4$ tribochemical phase,

shown by the Raman spectra in Fig. 4.4(b). This oxide tribolayer provides wear resistance and minimizes plastic flow, unlike pure nickel where the oxide layer repeatedly delaminated during sliding. The WC particles in the coating facilitated the formation of the tribolayer causing less plastic deformation inside the Ni-WC wear track [27]. During 400°C sliding, as previously mentioned, the Ni coating and Ni-WC coating's wear rates increased while their CoF decreased. This trend, based on the SEM wear track images in Fig. 4.8, is due to a change in mechanisms from adhesive to oxidative wear. Figures 4.7(a,d) show low and higher magnification SEM images inside the Ni coating wear track during 400˚C sliding. The wear track in Fig. 4.7(a) exhibits patches of a smooth oxide tribolayer, or oxide glaze layer, formed on the surface along with slightly elevated lips on the sides of the wear track, which are both characteristic signatures of oxidative wear.

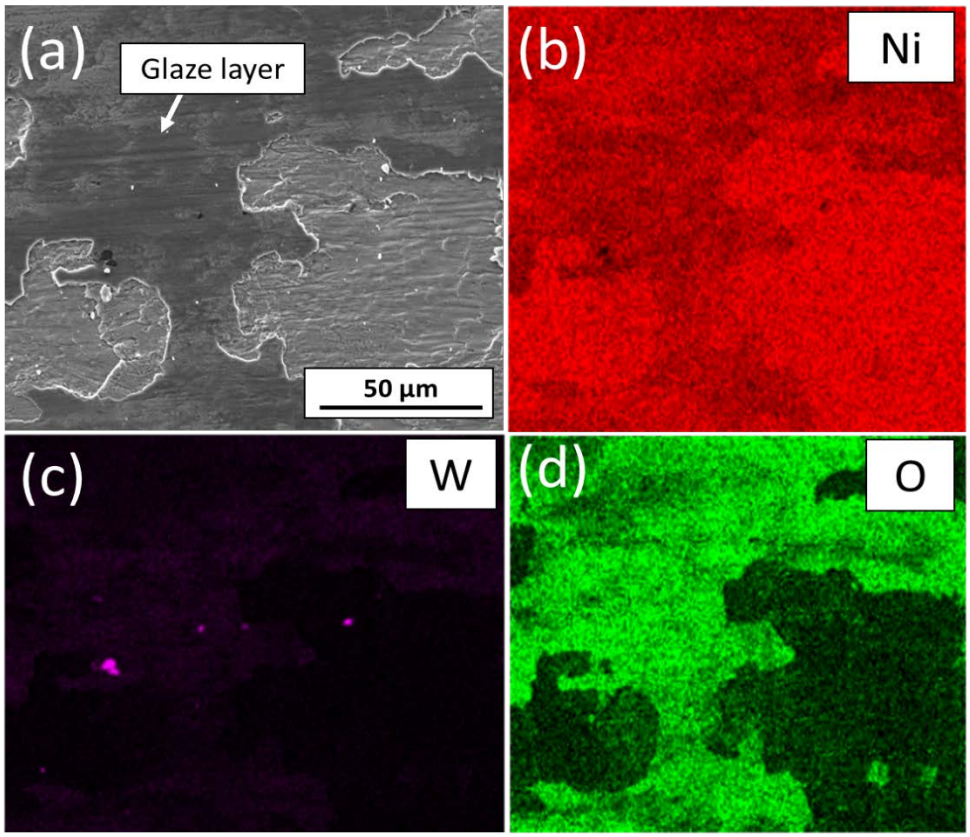

Figure 4.6: SEM image and corresponding EDS maps of the pure Ni wear track at RT.

The higher magnification image in Fig. 4.7(d), acquired from the box location in Fig. 4.7(a), shows the oxide tribolayer (white arrow) that forms from the compacted wear debris seen below the tribolayer. According to the Raman spectrum in Fig. 4.4(a), this is a predominantly NiO-containing tribolayer. These findings are in agreement with previous room temperature wear studies, indicating formation of a surface oxide glaze layer [29-32]. However, unlike room temperature sliding, a higher wear rate was observed for these elevated temperatures, even with the formation of the oxide tribolayer. This may be explained by the aforementioned thermal softening of the cold sprayed Ni coating from RT to 400°C, in agreement with comparison of the increase in wear track widths between Figs. 4.5(a) and 4.7(a), respectively. Furthermore, due to the softening effect, the Ni coating during 400°C sliding becomes susceptible to plastic flow during the initial run-in period, shown by its high CoF in Fig. 4.3, where most of the wear likely occurs before forming a stable oxide tribolayer [27].

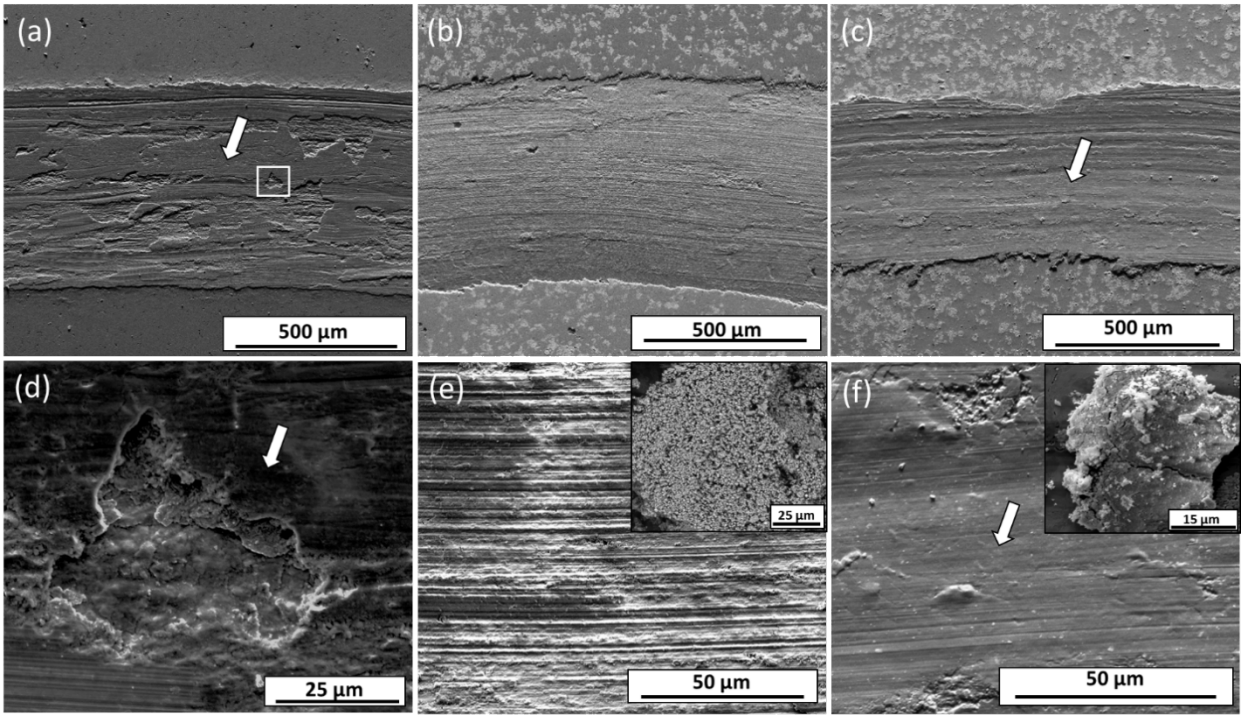

Figure 4.7: Low and higher magnification SEM wear track images on (a,d) Ni at 400°C, (b,e) Ni-WC at 200°C, and (c,f) Ni-WC at 400°C. Inset images in (e,f) show wear debris morphology outside the wear track. White arrows in (a,c,d,f) denote oxide-containing tribolayers formed at 400°C.

Figure 4.7 also shows low and higher magnification SEM images of the Ni-WC coating wear tracks during 200°C and 400°C sliding. Interestingly, a high degree of abrasive wear was observed in the 200°C Ni-WC coating wear track, shown in Figs. 4.7(b,e). The change in wear mechanisms from RT to 200°C is attributed to the Ni matrix softening during annealing thereby weakening the cohesion between the Ni matrix and WC particles. Therefore, the more highly stressed carbide particles were likely ejected at a higher rate under these conditions. This allowed for ploughing wear and the formation of fine oxides particles. The generated wear debris, such as the inset SEM image shown in Fig. 4.7(e), was then recycled through the mating interface leading to abrasive wear as the particles were dragged through the sliding contact. These oxide particles were continuously re-fractured into finer debris at the sliding interface and contributed to increasing abrasive wear. Moreover, oxide particles detached from the unstable tribolayer act as third-body abrasive particles on softened Ni and oxide film. Guo et al. [36] found similar results due to the inhomogeneity of WC-Ni ceramic phase in a NiCrBSi/WC-Ni composite coating that resulted in severe shear removal of WC particles creating third-body abrasive wear, contributing to the higher friction observed at elevated temperatures for the composite coatings. Since the 200°C temperature was not high enough to sinter the oxide particles together [31], a well-adhered and protective oxide tribolayer never fully formed during sliding. Instead, thermal softening dominates, leading to higher adhesion of Ni matrix, and thus both the CoF and wear rate increased significantly (Table 4.3 values). Figs. 4.7(c,f) show low and higher magnification SEM images of the Ni-WC coating wear tracks during 400°C sliding. Unlike during 200°C sliding, the 400°C environment was high enough to eventually promote the formation of a protective oxide NiO-rich tribolayer, according to the Raman spectrum in Fig. 4.4(b), which mitigated both the CoF and wear rate (Table 4.3 values). The mechanically mixed oxide tribolayer, denoted by the white arrows in

Figs. 4.7(c,f), is more continuous across the entire wear track in comparison to the RT wear track in Figs. 4.7(a,d), and it mitigated the abrasive wear that occurred in the 200˚C wear track in Figs. 4.7(b,e). In addition, the wear track width at 400°C, shown in Fig. 4.7(c), is clearly smaller than the wear track width at 200°C sliding, shown in Fig. 4.7(b). This change in wear mechanisms is further shown in Fig. 4.8 where the brighter contrast phase corresponds to WC particles. It is apparent that the distribution of WC particles is more homogenous at 200°C, while at 400°C the WC particles at the surface are diminish due to the formation of the lubricious NiO layer. At 200°C, the thermal softening facilitates loose WC particle that readily eject at the sliding interface, leading to (fine) fragmented WC in the worn surface characterized by microcutting in Fig. 4.8(c).

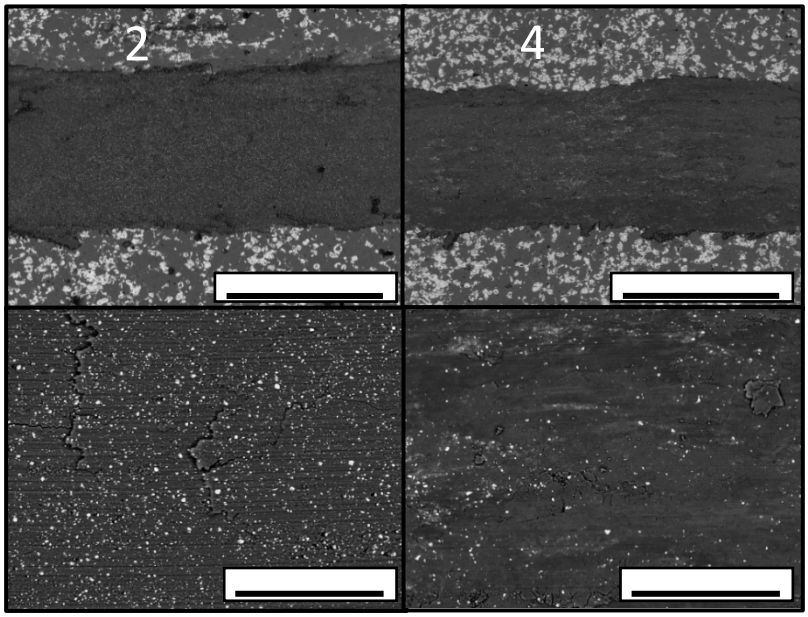

Figure 4.8: Backscattered images of worn surface morphology for the Ni-WC coating at (a,c) 200˚C and (b,d) 400˚C

There is also an accompanying change in wear debris morphology between 200°C and 400°C sliding. The inset SEM image in Fig. 4.7(f) shows that the 400°C generated wear debris exhibits a smoother, plate-like structure. Similar to the aforementioned thermal softening of the Ni coating from RT to 400°C, there is an increase in wear track widths on the Ni-WC coating, shown by

comparing Figs. 4.5(b) and 4.7(c) images, respectively. Likewise, due to the softening effect, the Ni-WC coating during 400°C sliding becomes susceptible to plastic flow during initial run-in period (see Fig. 4.3) where most of the wear likely occurs, which also indicates that a surface adaption interval is required for forming a stable NiO tribolayer. Regardless of thermal softening and initial run-in higher wear, both CoF and wear rate are slightly lower for the Ni-WC coating compared to the Ni coating (Table 4.3 values).

Figure 4.9 shows optical microscopy images of the WC-Co counterfaces and corresponding Raman spectra acquired on the counterfaces after sliding on the Ni-WC coating during RT and 400°C sliding. It is evident from Fig. 4.9(a) that after RT sliding the ejected wear debris on the WC-Co counterface is composed of NiO, WO_3, and $NiWO_4$, which are the same tribochemical phases present on the wear track surfaces, as shown in Fig. 4.4(b). Also, a small amount of amorphous C was detected in some of the ejected wear debris, denoted by blue arrow in Fig. 4.9(a). The optical image in Fig. 4.9(a) clearly shows the counterface exhibits a wear flat and Raman spectroscopy analysis determined that there is no evidence of an oxide containing transfer film on the counterface. In contrast, the optical image and Raman spectrum in Fig. 4.9(b) shows that during 400°C sliding the presence of a NiO transfer film adhered to the counterface. The same NiO tribolayer formed inside the Ni-WC wear track at 400°C, shown in Fig. 4.4(b). This self-mating tribolayer is responsible for the reduced CoF and wear rate during 400°C sliding. Similarly, Hager et al. [32] reported a noticeable drop in CoF at 300°C between Ti-6Al-4V and cold sprayed Ni due to the formation of a coherent transfer film, along with in the transformation of Ni_2O_3 into the more thermodynamically favored NiO phase under those conditions. Previous studies reported that the same lubricious NiO transfer film formed in Ni-based coatings resulting in reduced CoF values [30-35].

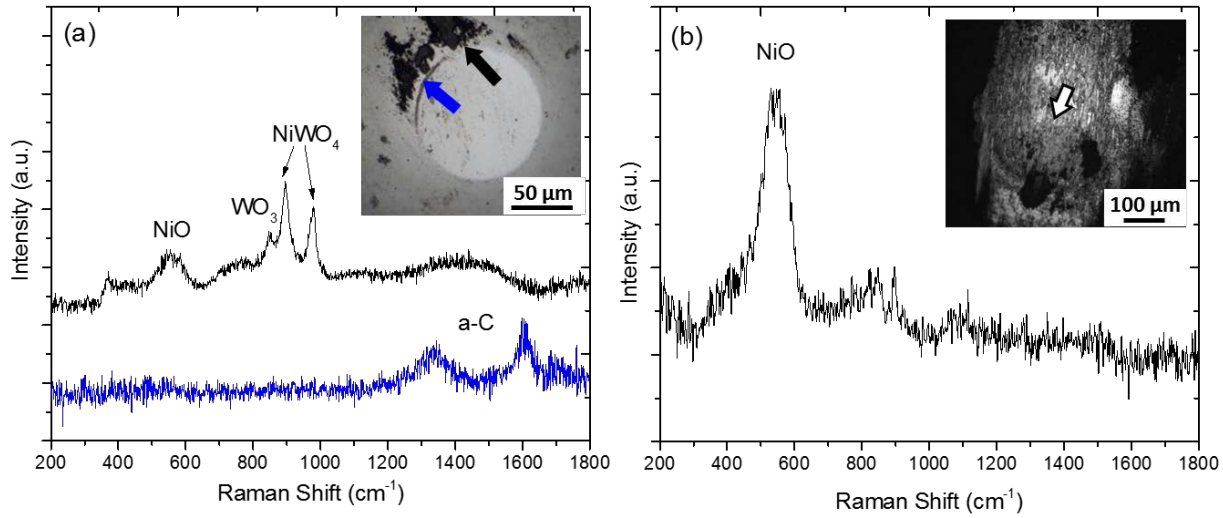

Figure 4.9: Raman spectra of wear debris and transfer film on the WC-Co counterface after sliding on Ni-WC coating at (a) RT and (b) 400°C. The arrows in the optical microscopy images denote the chemical phases in the Raman spectra.

To further understand the adaptive friction behavior of the Ni-WC coating at elevated temperatures, sliding wear tests were conducted by in situ thermal cycling between RT and 400°C. Figure 4.10 shows the dynamic CoF behavior starting and ending at RT with two thermal cycles to 400°C. It is evident that the Ni-WC coating exhibits self-adaptive friction behavior when comparing to the static CoF values listed in Table 4.3. Initially, the RT CoF was ~0.4, in agreement with the static CoF value of 0.41 during RT sliding. Interestingly, during the first thermal cycle, the CoF decreased to ~0.2 between ~200°C to 300°C, which is much lower than the static 200°C CoF of 0.59. This lowering of friction shortly lasted as the friction successively increased to ~0.6 suggesting a transition occurred from oxidative wear (tribolayer formation) to adhesive/abrasive wear (thermal softening), as explained previously in the static tests of cold sprayed Ni-WC. With further heating to 400°C during the first thermal cycle, the CoF decreased to ~0.3 in agreement with the static CoF value. Subsequent thermal cycling showed that this initial period of low CoF at ~0.2 did not occur again, whereas the dynamic CoF values agreed with the static CoF values for the remainder of the test to 350 m sliding distance.

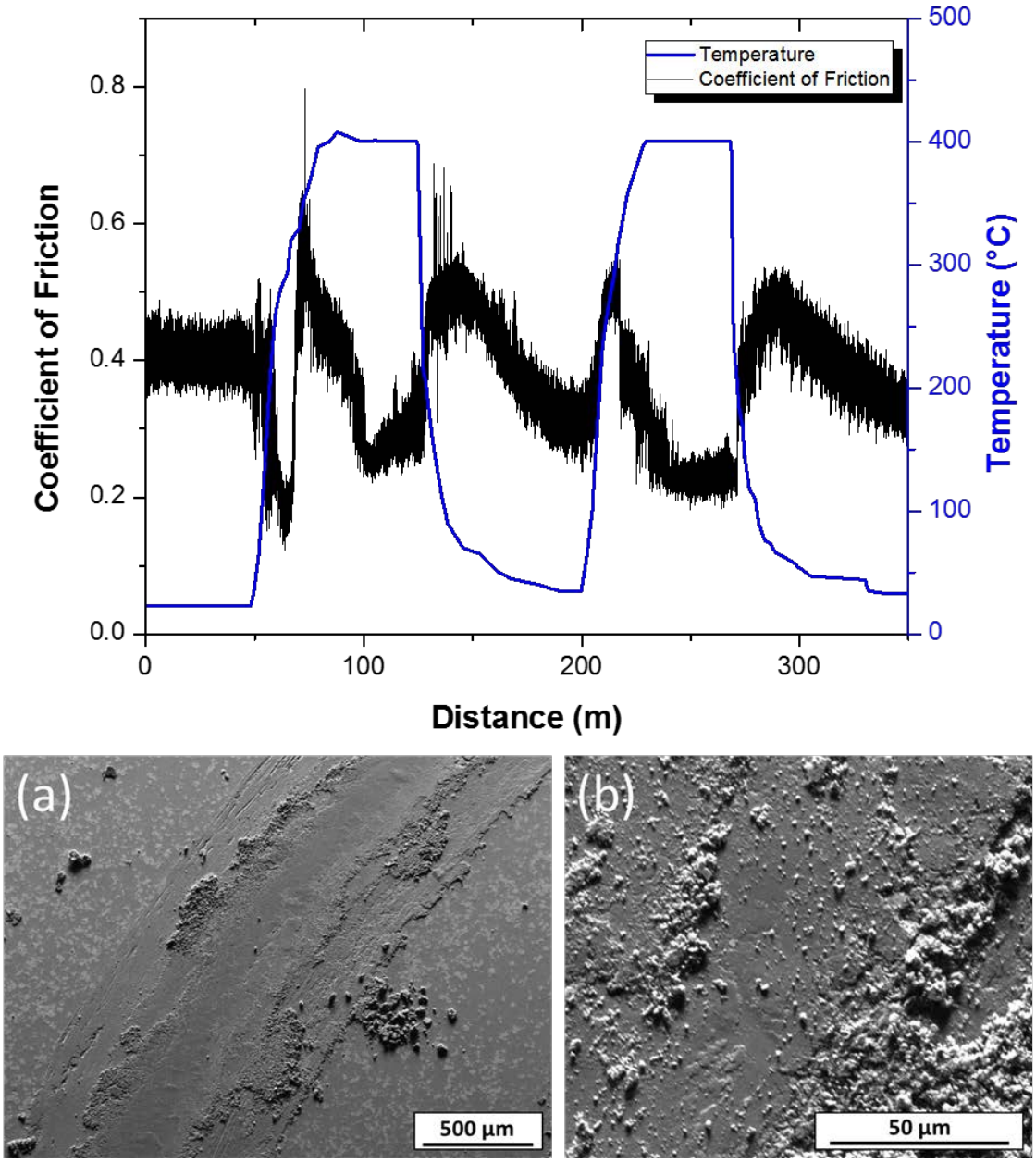

Figure 4.10: Thermal cycle friction behavior of Ni-WC coating. SEM images of wear track at (a) low and (b) high magnifications.

The initial drop in CoF values for pure Ni coating has been explained by the enhanced plasticity and a reduction in the ratio of Ni_2O_3 to NiO in the wear track [31-33]. However, as the temperature-actuated oxidation progressed, the increase in the CoF occurred as the formation in the compacted oxide layer was contributing to abrasive wear until the oxidative wear and glaze formation became more predominant to gradually reduce friction. Low and higher magnification SEM images of the

thermal cycled wear track are shown in Figs. 4.10(a,b). There are large amounts of submicron debris formed from ploughing through the stable oxide layer [34]. The friction reduction is due to the replenishing of this submicron debris that facilitates the formation of a stable, compacted lubricious oxide layer at a faster rate. Overall, the thermal cycle test confirms that a cold sprayed Ni-30 vol. % WC is an effective self-adaptive coating for fiction behavior.

CHAPTER 5

SUMMARY AND CONCLUSION

A Ni-WC composite coating was fabricated using CS processing to study the processing-structure-tribological property relationship, specifically at elevated temperatures. The Ni-WC composite coating was selected based on the known wear performance exhibited by Ni-WC coatings using thermal spray and vapor deposition processes. Through SEM and EDS, XRD, and Raman spectroscopy analysis, the tribological properties and mechanisms were investigated to provide a fundamental mechanistic insight into the coat's friction and wear behavior at elevated temperatures. Below are the major conclusion taken away from the project:

- Cold spray Ni-WC composite coatings have improved friction behavior and wear resistance at RT and 400˚C when compared to pure Ni cold spray coatings.
- Unidirectional dry sliding resulted in lower COF values with increased temperature due to a change in wear mechanisms and mechanical properties, however there are higher wear rates at 400°C due to the thermal softening of the Ni matrix.
- Raman spectroscopy revealed the formation a NiO 'glaze' at higher temperatures along with the formation of a lubricious, self-mating NiO transfer film. The transfer film and 'glaze' layer were associated with the reduction in friction.
- The coating exhibited self-adaptive friction behavior upon temperature cycling.
- While thermal softening at elevated temperatures slightly compromised the wear resistance, the formation of the lubricious tribofilm was advantageous in reducing friction.
- Therefore, the CS Ni-WC composite coatings deposited on steel could potentially be used for high temperature bearing cages that still require the need for high temperature solid lubricants.

CHAPTER 6

RECOMMENDATIONS FOR FUTURE WORK

Based on the results presented in this thesis, future work and studies are recommended to:

- Investigate the effects of different counterfaces such as steel or Si_3N_4 to ascertain further insight into the wear mechanism of the lubricious NiO phase at elevated temperatures.

- Conduct intermediate, higher temperature (above 400°C) and subsequent thermal cycling tests on the Ni-WC composite to further understand the wear and growth mechanisms of NiO in conjunction with thermal softening of the Ni matrix.

- Determine the optimal gas temperature to obtain advantageous tribological properties (i.e. wear resistance and low friction) by manipulating the volume faction of deposited secondary particles.

- Perform more detailed mechanistic studies of the lubricating surface at elevated temperatures with the use of XPS, FIB/SEM and cross sectional TEM analyses.

REFERENCES

[1] B. Bhushan. Modern Tribology Handbook. Boca Raton, FL: CRC, 2001.

[2] G.W. Stachowiak. Wear -Materials, Mechanisms and Practice. Chichester, England: Wiley, 2005.

[3] Holmberg, Kenneth, and Allan Matthews. Coatings Tribology: Properties, Mechanisms, Techniques and Applications in Surface Engineering. Amsterdam: Elsevier, 2009.

[4] T.W. Scharf and S.V. Prasad. “Solid Lubricants: a review”. J. Matr. Sci.48 (2013): 511-531.

[5] Dowson, Duncan. History of Tribology. 6th ed. Vol. 50. London: Professional Engineering, 1998.

[6] A. Matthews, S. Franklin and K. Holmberg. “Tribological coatings: contact mechanisms and selection”. J. Phys. D: Appl. Phys. 40 (2007): 5463-75.

[7] S.M. Aouadi, H. Gao, A. Martini, T.W. Scharf, and C. Muratore. "Lubricious Oxide Coatings for Extreme Temperature Applications: A Review". Surf. Coat. Techno. 257 (2014): 266-77.

[8] T.W. Scharf, S.V. Prasad, P.G. Kotula, J.R. Michael, and C.V. Robino. "Elevated Temperature Tribology of Cobalt and Tantalum-based Alloys". Wear 330-331 (2015): 199-208.

[9] R.R. Chromik, H. W. Strauss, and T. W. Scharf. "Materials Phenomena Revealed by In Situ Tribometry." JOM 64 (2012): 35-43.

[10] A. Moridi, S. M. Hassani-Gangaraj, M. Guagliano, and M. Dao, Cold Spray Coating: Review of Material Systems and Future Perspectives. *Surf. Eng*. 30 (2014) 369-95.

[11] R.C. Dykhuizen and M.f. Smith, Gas Dynamic Principles of Cold Spray, *J Ther. Spray Techno.* 7 (1998) 205-12.

[12] J.R. Davis, Handbook of Thermal Spray Technology, ASM international, 2004.

[13] T.W. Clyne and P. J. Withers, An Introduction to Metal Matrix Composites. Cambridge: Cambridge UP, 2003.

[14] R.R. Chromik, S.A. Alidokht, J. Michael Shockley, and Y. Zhang, Tribological Coatings Prepared by Cold Spray. Cold-Spray Coatings (2017) 321-48.

[15] K. Kato, Wear in Relation to Friction- a review. *Wear.* 241 (2000) 151-57.

[16] F. Gartner, T. Stoltenhoff, T. Schmidt, and H. Kreye, The Cold Spray Process and Its Potential for Industrial Applications. *J Ther. Spray Techno.* 15 (2006) 223-32.

[17] A. A. Voevodin and J. S. Zabinski, Supertough Wear Resistant Coatings with “Chameleon” Surface Adaptation. *Thin Solid Films*. 370 (2000) 223-231.

[18] C. Muratore and A.A. Voevodin, Chameleon coatings: adaptive surfaces to reduce friction and wear in extreme environments. Annual Reviews of Materials Research. 39 (2009) 11.1-11.28

[19] A.A.Voevodin, C. Muratore, S.M.Aouadi, Hard Coatings with High Temperature Adaptive Lubrication and Contact Thermal Management: Review. *Surf.Coat. Techno*. 257 (2014) 247-265.

[20] S. M. Aouadi, H. Gao, A. Martini, T. W. Scharf, C. Muratore, Lubricious oxide coatings for extreme temperature applications: A review. *Surf. Coat. Techno.* 257 (2014) 266-277

[21] J. Michael Shockley, E.F. Rauch, R.R. Chromik, and S. Descartes, TEM Microanalysis of Interfacial Structures after Dry Sliding of Cold Sprayed Al-Al 2 O 3. *Wear.* 376-377 (2017): 1411-417.

[22] Y. Zhang, Y. Epshteyn, and R.R. Chromik, Dry Sliding Wear Behaviour of Cold-sprayed Cu-MoS 2 and Cu-MoS 2 -WC Composite Coatings: The Influence of WC. *Tribo. Intern.* (2017).

[23] M. Rombouts, R. Persoons, E. Geerinckx, R. Kemps, M. Mertens, W. Hendrix, and H. Chen, Development and Characterization of Nickel Based Tungsten Carbide Laser Cladded Coatings. *Phy. Procedia*. 5 (2010) 333-39.

[24] K. Van Acker, D. Vanhoyweghen, R. Persoons, and J. Vangrunderbeek. Influence of Tungsten Carbide Particle Size and Distribution on the Wear Resistance of Laser Clad WC/Ni Coatings *Wear* 258 (2005) 194–202.

[25] J.S. Xu, X.C. Zhang, F.Z. Xuan, Z.D. Wang, and S.T. Tu, Microstructure and Sliding Wear Resistance of Laser Cladded WC/Ni Composite Coatings with Different Contents of WC Particle. *J.Mater. Eng. Perform.* 21 (2011) 1904-911.

[26] M.R. Fernández, A. García, J.M. Cuetos, R. González, A. Noriega, M. Cadenas, Effect of actual WC content on the reciprocating wear of a laser cladding NiCrBSi alloy reinforced with WC. *Wear.* 324–325 (2015) 80–89.

[27] S.A. Alidokht, P. Manimunda, P. Vo, S. Yue, and R.R. Chromik, Cold Spray Deposition of a Ni-WC Composite Coating and Its Dry Sliding Wear Behavior." *Surf. Coat. Techno.* 308 (2016) 424-34.

[28] J. Jiang, F.H. Stott, and M.M. Stack, The Role of Triboparticulates in Dry Sliding Wear. *Tribo. Intern.* 31 (1998) 245-56.

[29] F.H. Stott and G.C. Wood, The Influence of Oxides on the Friction and Wear of Alloys. *Tribo. Intern.* 11 (1978) 211-18.

[30] F.H. Stott, D.S. Lin, and G.C. Wood, The Structure and Mechanism of Formation of the 'Glaze' Oxide Layers Produced on Nickel-based Alloys during Wear at High Temperatures." *Corr. Sci.* 13 (1973) 449-69.

[31] J. Jiang, F.H. Stott, and M.M. Stack, Some Frictional Features Associated with the Sliding Wear of the Nickel-base Alloy N80A at Temperatures to 250°C. *Wear.* 176 (1994) 185-94.

[32] C.H. Hager, J. Sanders, S. Sharma, A.A. Voevodin, and A. Segall, The Effect of Temperature on Gross Slip Fretting Wear of Cold-sprayed Nickel Coatings on Ti6Al4V Interfaces. *Tribo. Intern.* 42 (2009) 491-502.

[33] C.H. Hager, J. Sanders, S. Sharma, and A.A. Voevodin, The Use of Nickel Graphite Composite Coatings for the Mitigation of Gross Slip Fretting Wear on Ti6Al4V Interfaces. *Wear.* 267 (2009) 1470-481.

[34] C.H. Hager, J. Hu, C. Muratore, A.A. Voevodin, and R. Grandhi, The Mechanisms of Gross Slip Fretting Wear on Nickel Oxide/Ti6Al4V Mated Surfaces. *Wear.* 268 (2009) 1195-204.

[35] W. Li, C. Huang, M. Yu, D. Liu, Y. Feng, and H. Liao, Investigation of High Temperature Oxidation Behavior and Tribological Performance on Cold Sprayed Nickel-alumina Composite Coating. *Surf. Coat. Techno.* 239 (2014) 95-101.

[36] C. Guo, J. Zhou, J. Chen, J. Zhao, Y. Yu, and H. Zhou, High Temperature Wear Resistance of Laser Cladding NiCrBSi and NiCrBSi/WC-Ni Composite Coatings. *Wear.* 270 (2011) 492-98.

[37] S. Chan, In Situ Laser Raman Spectroscopy of Nickel Oxide Supported on Gamma-Al2O3. *J. Catalysis.* 103 (1987) 224-27.

[38] N. Mironova-Ulmane, A. Kuzmin, I. Steins, J. Grabis, I. Sildos, and M. Pars. "Raman Scattering in Nanosized Nickel Oxide NiO." *J. Phy.*: Conference Series 93 (2007)

[39] S. A. Alidokht, P. Vo, S. Yue, and R. R. Chromik, "Cold Spray Deposition of Ni and WC-Reinforced Ni Matrix Composite Coatings," *J Ther. Spray Techno.* 26 (2017) 1908-1921.

[40] M. Surender, B. Basu, and R. Balasubramaniam. "Wear Characterization of Electrodeposited Ni-WC Composite Coatings." *Tribo. Intern.* 37 (2004): 743-49.